Bulletin of the Seismological Society of America, 92, 1, pp. 172–193, February 2002

Dynamics of İzmit Earthquake Postseismic Deformation and Loading of the Düzce Earthquake Hypocenter

by Elizabeth Harding Hearn, Roland Bürgmann, and Robert E. Reilinger

Abstract We have developed dynamic finite-element models of İzmit earthquake postseismic deformation to evaluate whether this deformation is better explained by afterslip (via either velocity-strengthening frictional slip or linear viscous creep) or by distributed linear viscoelastic relaxation of the lower crust. We find that velocity-strengthening frictional afterslip driven by coseismic shear stress loading can reproduce time-dependent Global Positioning System data better than either linear viscous creep on a vertical shear zone below the rupture or lower crustal viscoelastic relaxation. Our best frictional afterslip model fits the main features of postseismic slip inversions, in particular, high slip patches at (and below) the hypocenter and on the western Karadere segment, and limited afterslip west of the Hersek Delta (Bürgmann *et al.,* 2002). The model requires a weakly velocity-strengthening fault, that is, either low effective normal stress in the slipping regions or a smaller value for the parameter describing rate-dependence of friction (a-b) than is indicated by laboratory experiments.

Our best afterslip model suggests that the Coulomb stress at the Düzce hypocenter increased by 0.14 MPa (1.4 bars) during the İzmit earthquake (assuming right-lateral slip on a surface dipping 50° to the north), and by another 0.1 MPa during the 87 days between the İzmit and Düzce earthquakes. In the Marmara Sea region (within about 160 km of the İzmit earthquake rupture), this model indicates that the Coulomb stresses increased by 15%–25% of the coseismic amount during the first 300 days after the earthquake. Three hundred days after the earthquake, postseismic contributions to Coulomb stressing rate on the Maramara region faults had fallen to values equal to or less than the inferred secular stress accumulation rate. Our estimates of postseismic Coulomb stress are highly model dependent: in the Marmara region, the linear viscous shear zone and viscoelastic lower crust models predict greater postseismic Coulomb stresses than the frictional afterslip model.

Near-field stress and fault-zone rheology estimates are sensitive to the Earth's elastic structure. When a layered elastic structure is incorporated in our model, it yields a Coulomb stress of 0.24 MPa at the Düzce hypocenter, significantly more than the 0.14 MPa estimated from the uniform elastic model. Because of the higher near-field coseismic stresses, the layered elastic model requires a higher value of velocity-strengthening parameter (A-B) ([a-b] times effective normal stress σ') to produce comparable postseismic slip. (A-B) is estimated at 0.4 and 0.2 MPa, respectively, for the layered and uniform elastic models. These results highlight the importance of understanding the Earth's elastic structure and the mechanism for postseismic deformation if we wish to accurately model coseismic and postseismic crustal stresses.

Introduction

The 17 August 1999 M_w 7.5 İzmit, Turkey, earthquake was followed by an observable, transient deformation of the Earth's surface within about 100 km of the rupture (Reilinger *et al.,* 2000). By the time of the M_w 7.1 Düzce event, 87 days later, this postseismic deformation had released an equivalent of 20% of the estimated coseismic moment (4.5

$\times 10^{19}$ N m, assuming the shear modulus (G) is 30 GPa); (Bürgmann *et al.,* 2002). Only about 5% of this moment can be attributed to aftershocks (Reilinger *et al.,* 2000).

In a companion article, Bürgmann *et al.* (2002) have modeled this surface deformation kinematically by inverting for afterslip in a uniform elasticity half-space. Their time-dependent inversions show significant slip on the rupture surface as well as below it, with maxima at the hypocenter and on the western Karadare segment (both areas of low coseismic slip). They also found that shallow postseismic slip decays more rapidly with time than deeper slip, and that very little afterslip occurs on the Yalova segment (i.e., the westernmost 25 km of the rupture).

In this article, we present three-dimensional, dynamic finite-element models of the postseismic deformation of the İzmit earthquake prior to the 12 November 1999 Düzce event. We focus on afterslip via either linear viscous creep or stable (velocity-strengthening) frictional slip in areas that were coseismically loaded. One objective of our modeling is to characterize the dynamics of the earthquake cycle on this segment of the North Anatolian Fault Zone (NAFZ); that is (1) to find the fault-zone material properties that best reproduce horizontal Global Positioning Data (GPS) data and postseismic slip history, and (2) to evaluate which mechanism is more geologically feasible. Another objective of our modeling is to estimate time-dependent postseismic stress change on nearby faults and to evaluate how well we can constrain stress evolution on these faults with the available GPS measurements. Using our best afterslip model, we predict time-dependent stress changes at the Düzce hypocenter and on faults in the Marmara Sea region. We also run forward models to evaluate how well our models reproduce continuous GPS displacements from stations west of the hypocenter for up to 300 days after the İzmit earthquake.

Model Mesh and Method

We calculate lithosphere stresses and displacements as a function of time using the three-dimensional viscoelastic finite-element code, GAEA (Saucier and Humphreys, 1993). This program solves for nodal displacements by balancing applied and internal elastic stresses after each time step, using a variational approach in which strain energy is minimized with respect to displacements. For elasticity problems, this method is equivalent to the engineering stiffness approach (Vichnevetsky, 1981). The GAEA code uses a Galerkin weighted residual method with quadratic block elements (three nodes per side), which allows smoothly varying fault surface geometry and slip to be represented without discontinuities. The three-dimensional finite-element mesh covers an 800- by 800-km region and is 200 km thick. It is aligned with its sides oriented E–W and N–S and is approximately centered on the Düzce and İzmit ruptures (Fig. 1). The crust is represented with five 6-km-thick layers of elements (i.e., a vertical nodal spacing of 3–6 km), and the mantle below is represented with elements of increasing thickness. Model elements are 6–10 km in horizontal dimension near the rupture traces (nodal spacing of 3–10 km) and expand in dimension with distance.

For reasons given in the Coseismic Model section, we model two elastic structures. The first is a uniform elastic model, as used by Bürgmann *et al.* (2002), with shear modulus G equal to 30 GPa and Poisson's ratio (ν) equal to 0.25. For comparison, we also model a layered elastic structure based on the CRUST 5.1 model (Mooney *et al.,* 1998) and local upper mantle V_p data from western Turkey (Mindavelli and Mitchell, 1989; Saunders *et al.,* 1998). For this model, shear modulus values of 30, 45, and 75 GPa are used for the upper crust (0–18 km), lower crust (18–30 km), and mantle, respectively. The minimum vertical element dimension (6 km) does not permit us to model a thin layer of low-G sediments at the surface, which may affect our ability to model station displacements within a few kilometers of the fault. All layers are modeled as Poisson solids (with Poisson's ratio $\nu = 0.25$), except in models where we vary ν to simulate poroelastic rebound. In our poroelastic models, we assume that the undrained value of ν in the upper crust is 0.28.

Coseismic slip (Reilinger *et al.,* 2000) is interpolated at the fault node coordinates for our mesh and is imposed using the split node technique (Melosh and Raefsky, 1981). The side and bottom boundaries of the model are fixed, and the surface boundary is unconstrained.

Afterslip Modeling

We model afterslip by calculating the horizontal shear stresses resolved onto planes tangent to the fault surface at each node and using a constitutive relationship (either linear viscous creep or velocity-strengthening frictional slip) to calculate the horizontal slip increment during each time step. This slip increment is added to the cumulative slip displacement for each split node and the sum is imposed for the following time interval.

Velocity-dependent frictional afterslip may be either stable or unstable, depending on the properties of the fault surface, temperature, and other parameters. The change in friction coefficient with slip velocity is parameterized with the value (a-b). If (a-b) is positive, the fault zone is velocity-strengthening and slip is stable. If (a-b) is negative, the fault zone is velocity-weakening and there is an occurrence of stick-slip behavior. Velocity-strengthening frictional afterslip may occur on the earthquake rupture surface in areas of low coseismic slip, where the fault zone was loaded during the earthquake (Marone *et al.,* 1991). At depths of less than about 4 km and greater than about 11 km, laboratory data suggest that typical continental faults may be velocity-strengthening and creep throughout the earthquake cycle (e.g., Stesky, 1978; Blanpied *et al.,* 1991, 1995). Parts of the fault surface that exhibit stick-slip behavior during most of the earthquake cycle, may also become velocity-strengthening temporarily after an earthquake, possibly as a result of gouge creation, shear heating, or some other process. In either case, we assume velocity-strengthening friction to

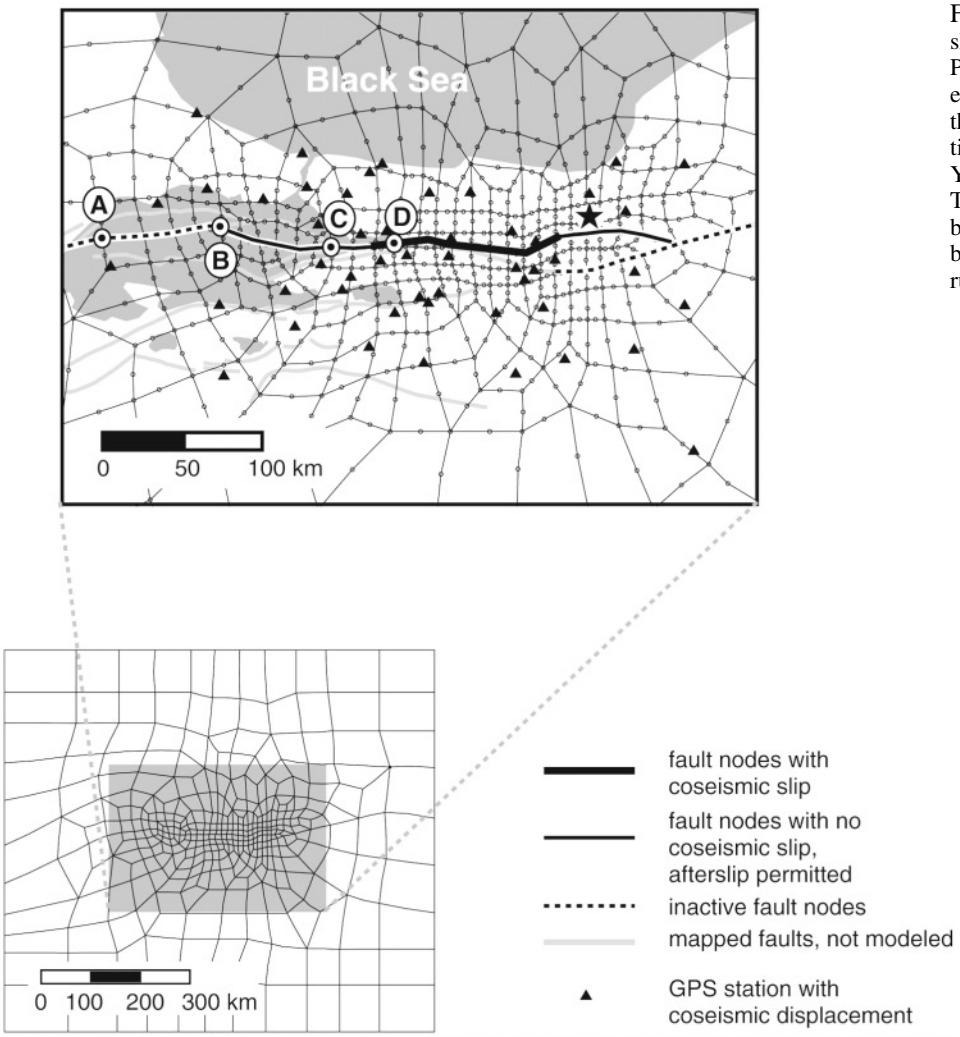

Figure 1. Model mesh. The top figure shows a close-up, centered on the İzmit region. Points A, B, and C are Marmara Sea fault reference locations 160, 100, and 20 km west of the end of the İzmit surface rupture, respectively. Point D is a reference location on the Yalova fault segment, 20 km from its west end. The star marks the epicenter of the 12 November 1999 Düzce earthquake, and the heavy black line marks the 1999 İzmit earthquake rupture.

model postseismic slip on all parts of the İzmit rupture that were loaded during the earthquake, as well as at depths exceeding 15 km. We calculate slip during each time step using the following equation (Marone *et al.,* [1991], derived from the equations of Dieterich [1979], or Ruina [1983]).

$$\mathrm{d}s = \mathrm{d}t\, V_0 \exp\left(\frac{\cdot\tau}{(a-b)\sigma_n'}\right) \qquad (1)$$

V_0 is the secular slip rate, (a–b) is an empirical constant relating fault friction change to change in slip velocity, σ_n' is the effective normal stress, ds is the slip per time step, dτ is the time-dependent earthquake-related shear stress resolved onto the fault surface, and dt is the time-step length (1–10 days). This method for modeling stable frictional afterslip is similar to the hot friction approach used by Linker and Rice (1997) to model afterslip following the 1989 Loma Prieta, California, earthquake.

Equation (1) assumes that steady-state friction is attained during coseismic slip wherever afterslip is modeled. This means that coseismically, we assume the fault surface slipped by at least the critical slip distance D_c from frictional slip theory (Dieterich, 1979; Ruina, 1983). D_c in the crust has been estimated at 1–10 mm (Marone *et al.,* 1991) or far less (tens of microns, Blanpied *et al.,* 1995, 1998). In locations where coseismic slip is less than D_c (i.e., at depth below the rupture, or off the fault ends), we may overestimate the rate of slip before D_c is attained because equation (1) does not account for time-dependent drop in the coefficient of friction during slip for distances less than D_c. The effect of this assumption is probably minor unless D_c is much larger than 1–10 mm.

In our modeling, V_0 is fixed at 20 mm/yr, approximately consistent with the long-term slip rate for the North Anatolian Fault (NAF) in western Turkey (e.g., Straub *et al.,* 1997; McClusky *et al.,* 2000; Meade *et al.,* 2002). We vary the parameter (A-B) = (a-b) σ_n'. This parameter increases with depth in the crust (σ_n' increases with depth and (a-b) increases with temperature and thus depth), but the form of this depth dependence in the Earth is not well constrained. For simplicity, we focus on models with uniform (A-B) on the postseismically slipping surface. We also run a set of

models in which (*A*-*B*) is constant from 0 to 15 km depth, then increases linearly to 10 times its upper crustal value over the next 15 km depth interval. In all the velocity-strengthening frictional afterslip models, we model the upper 15 km of the NAFZ beyond the ends of the rupture as locked (i.e., velocity-weakening), with (*A*-*B*) below 15 km the same as below the ruptured segments.

For linear viscous shear zone creep, the slip (i.e., integrated shear strain across the deforming shear zone) per time step is calculated with equation (2).

$$ds = \frac{\delta\tau}{\left(\frac{\eta}{w}\right)} dt \tag{2}$$

In equation (2), η is the viscosity and w is the width of the shear zone. We vary the parameter (η/w), which is assumed to be uniform in our models. We also consider the effect of varying locking depth (i.e., depth below which viscous creep is permitted in the model) for the İzmit rupture and adjoining fault segments. The linear viscous creep model may be interpreted as representing shear zone deformation caused by linear viscous processes such as intergranular pressure solution creep or diffusion creep. This model may also represent nonlinear deformation in a shear zone, if postseismic shear stress change is small compared with pre-earthquake shear stress on the fault (i.e., the coseismic drop in effective viscosity of the shear zone is small).

Shallow Interseismic Creep and Our Afterslip Models

Postseismically slipping fault patches are loaded by the sum of earthquake-related (coseismic and postseismic) stress changes and pre-earthquake stress. Because stresses on the western NAFZ prior to the İzmit earthquake are not known, we model the rate of creep or slip in excess of the pre-earthquake rate, assuming that it depends solely on earthquake-related shear stress change. In taking this approach, we have built in some assumptions about the interseismic behavior of the NAFZ, particularly whether the postseismically slipping patches were slipping before the earthquake.

The evidence for or against interseismic slip on the NAFZ is vague. GPS data suggest that the NAFZ in the İzmit region was locked between 0 and 17 km depth before the İzmit earthquake, but there is a considerable uncertainty about this estimate (Meade *et al.,* 2002). The İzmit hypocenter was a hot spot for seismic activity for many years prior to the İzmit earthquake (Hubert-Ferrari *et al.,* 2001), but the small earthquakes could have been either at the boundaries of an asperity at the hypocenter (Honkura *et al.,* 2000; Onsel and Wyss, 2000) or seismicity associated with creep at the hypocenter (Reilinger *et al.,* 2000).

If creep occurred interseismically in locations where postseismic slip was also concentrated, our use of earthquake-related shear stress change (rather than total shear stress) in equations (1) and (2) is appropriate. If the NAFZ did not slip or creep interseismically above 17 km depth, however, total shear stress on the fault should be used in equation (2) to calculate the rate of any viscous shear zone creep at a depth of less than 17 km. Otherwise, our use of stress change rather than total stress in equation (2) would imply that shear stresses on the postseismically slipping patches was close to 0. Since this is likely untrue, in the event that the NAFZ was locked down to 17 km depth, our linear viscous shear zone models may underestimate shear zone viscosity.

A locked NAFZ down to 17 km depth, even with anomalously high stress at the hypocenter, is consistent with models of continental fault zones that are velocity strengthening below ca. 10 km depth. Such faults have retarded or negligible rates of slip above depths of 20–25 km late in the earthquake cycle (Tse and Rice, 1986; Lapusta *et al.,* 2000). (Nonslipping, velocity-strengthening fault patches could also be under higher stress than adjoining parts of the fault, given a higher coefficient of friction.) Thus, even if the NAFZ was not creeping at depths less than 17 km before the earthquake, our calculation of frictional afterslip rate based on earthquake-related stress change (and $V_0 = 20$ mm/yr) should be appropriate.

Viscoelastic Relaxation and Poroelastic Rebound

It has been shown (in two dimensions) that viscoelastic relaxation of the horizontal layers may produce horizontal surface deformation identical to that resulting from afterslip (Savage and Prescott, 1978). Models of postseismic deformation following the 1992 Landers earthquake (e.g., Savage and Svarc, 1997; Pollitz *et al.,* 2000) suggest that the two processes can yield similar horizontal surface deformation in the three-dimensional case as well. We have developed models of linear viscoelastic relaxation of the lower crust to evaluate whether this process, rather than frictional afterslip or linear viscous fault-zone creep, could be responsible for an early İzmit earthquake postseismic deformation. Viscoelastic relaxation of crustal layers is modeled automatically by the finite-element code when both elastic parameters and a viscosity are specified. GAEA calculates elastic stresses after each time step throughout the modeled volume. In elements where a viscosity is specified, viscous deformation over the time step interval is also calculated, and the resulting nodal displacements are effectively imposed for the following time step. In these models, we vary viscosity in the lower crust (24–30 km depth) where temperatures are highest, and we infer that crustal viscosity is at a minimum. On the basis of our experience, modeling viscoelastic layers in the lower crust or upper mantle (rather than in the middle crust) gives us the best chance of producing a long wavelength, temporally rapidly decaying transient of the appropriate magnitude.

We have also developed a simple model to evaluate whether poroelastic rebound contributes significantly to an early postseismic deformation following the İzmit earthquake, as it might have after the 1992 Landers, California,

earthquake (Peltzer *et al.,* 1998). Poroelastic rebound occurs when the compressibility of permeable, water-bearing crustal layers increases with time after an earthquake, causing the crust to expand or contract continuously. Total poroelastic surface deformation may be estimated by calculating surface displacements for elastic models with poroelastic layers that are undrained (less compressible, coseismic condition) and drained (more compressible, postseismic condition after coseismic water pressure gradients have vanished) and differencing the two solutions (e.g., Roeloffs, 1996; Peltzer *et al.,* 1998). In our model, we assume that the undrained and drained Poisson's ratios are 0.28 and 0.25, respectively, and that poroelastic changes to the compressibility are significant in the upper 18 km of the crust.

Parameter Estimation

Using either a Monte Carlo or grid search approach, we invert for rheological parameters by minimizing the cumulative summed squared residual (SSR) between modeled and measured displacements at GPS stations. Residuals to the measured surface displacements at each GPS site are calculated at 10-day intervals between the İzmit and Düzce earthquakes; the sum of these residuals over eight intervals is the quantity that is minimized. At campaign mode GPS sites, where daily position data are not available, we interpolate displacements at the end of each 10-day period using summed exponential and linear functions (Ergintav *et al.,* 2002). Only GPS sites with three or more observations between the İzmit and Düzce events are used in the inversion. For the simple models presented in this study, only one parameter is formally estimated (η/w, [A-B], or lower crustal η). We also explore the effect of changes to locking depth for our linear viscous fault zone creep models by running three suites of models with locking depths set at 5, 10, and 20 km.

Coseismic Model

Before postseismic deformation can be dynamically modeled, an elastic model that accurately represents coseismic stress changes in the crust and upper mantle is required. Ideally, this model should incorporate a layered elastic structure representing continental lithosphere and a detailed, coseismic slip distribution obtained assuming this elastic structure. However, as we wish to compare our dynamically modeled slip to postseismic slip distributions that were estimated with an elastically uniform Earth model (Bürgmann *et al.,* 2002), we assume the same uniform elastic parameters ($G = 30$ GPa, $\nu = 0.25$) in our models. We address separately how using a layered elastic structure (described in the section Model Mesh and Method) affects estimates of coseismic and postseismic crustal stresses, and whether using such a model would alter our main conclusions.

Figure 2 shows modeled and measured coseismic surface displacements at most of the 51 GPS stations that were displaced by at least 3 mm during the earthquake. Our modeled displacements are similar (but not identical) to those reported by Reilinger *et al.* (2000), as both models assume the same elastic structure and similar coseismic slip. The sum of the squared residuals weighted by two times the formal one-sigma measurement errors (weighted residual sum of squares [WRSS]) is 9600. This represents a reduction of 96% in WRSS relative to a model in which surface displacements are zero at all GPS sites. Most of the misfit between the model and GPS data is in the near field and may arise because large, short-wavelength variations in the displacement field cannot be properly represented by our model mesh. In addition, near-field displacements are highly sensitive to small spatial variations in coseismic slip. When we interpolate coseismic slip from a segmented, linear rupture model (Reilinger *et al.,* 2000) to different nodal positions on our curvilinear modeled fault, some smoothing is introduced in the slip distribution and in the displacement field close to the fault.

Modeled coseismic shear stresses resolved onto the İzmit rupture surface (assuming horizontal slip vectors) are shown in Figure 3. At the hypocenter and at the west end of the Karadare segment, where patches of low coseismic slip are surrounded by areas of higher slip, the fault surface is loaded by up to 4 MPa. Shear stresses of up to 10 MPa occur locally beyond the rupture ends and at depth below the coseismic rupture. Coseismic shear stress drops are comparable in magnitude (about 5–10 MPa) at the high slip patches.

Effect of Layered Elastic Structure

When we impose the slip distribution, reported by Reilinger *et al.* (2000), on the layered elastic structure described in the Methods section, the fit to coseismic surface displacements is significantly degraded; the WRSS increases by a factor of 3. In particular, the layered elastic model yields smaller displacements (and a worse fit to measured displacements) in the intermediate to far-field. The differences between modeled and measured surface displacements are of the order of centimeters, and far exceed the two-sigma displacement measurement errors of nearly all GPS sites.

This result is not surprising. Many studies have shown that strike-slip dislocations in a layered elastic structure in which G increases with depth, produce more localized surface displacements than equivalent dislocations in a uniform half-space (e.g., Rybicki, 1971; Savage, 1987). To produce displacements comparable to those from a layered elastic dislocation model, a half-space elastic model requires a shallower dislocation depth (Savage, 1987). Thus, in order to reproduce the surface displacements of half-space elastic model, a realistic layered Earth model requires added slip at depth.

To evaluate how much added slip our layered elastic model needs to reproduce observed coseismic surface displacements, we invert these displacements for slip on a three-panel İzmit fault model, using both layered and uniform elastic models. We model uniform slip on the Golcuk, East and West Sapanca, and Karadare segments with panels

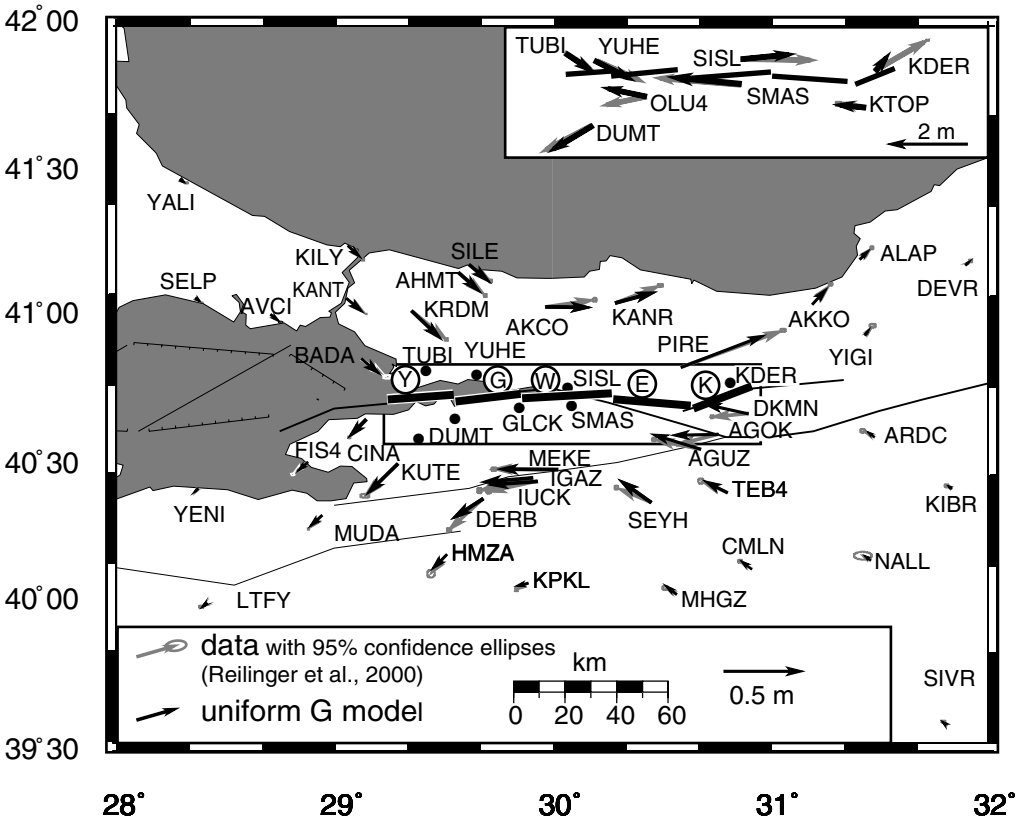

Figure 2. Modeled coseismic displacements and measured displacements as reported by Reilinger *et al.* (2000). Error ellipses show 95% confidence intervals. The model, shown with black arrows, assumes a uniform ($G = 30$ GPa, $\nu = 0.25$) elastic Earth and the coseismic slip distribution reported by Reilinger *et al.* (2000). Near-field displacement vectors are shown in the inset so that details in this area may be seen. Y, G, W, E, and K are the Yalova, Golcuk, West Sapanca, East Sapanca, and Karadare fault segments, respectively.

at 0–9, 9–18, and 18–24 km depths and use a Monte Carlo approach to solve for slip on these panels that minimizes the misfit between the modeled and measured surface displacements. Figure 4 illustrates how the summed squared misfit to coseismic displacements varies with the total moment of the modeled slip (assuming $G = 30$ GPa). The layered Earth model requires more slip to fit surface displacements as well as the uniform elastic model, and this added slip appears to be concentrated below 9 km. Admissible moments for the layered elastic model are about 30% greater than for the uniform elastic model. This finding is consistent with the fact that seismic moment estimates based on layered Earth models ($2.3–2.6 \times 10^{20}$ N m; Bouchon *et al.,* 2002; Delouis *et al.,* 2002; Gulen *et al.,* 2002) are about 25%–40% greater than geodetic moment estimates, which are based on a uniform elastic model with G equal to 30 GPa ($1.6–1.7 \times 10^{20}$ N m; Reilinger *et al.,* 2000; Feigl *et al.,* 2002).

We created hypothetical slip distributions with moments of 2.1×10^{20} and 2.5×10^{20} N m to see how well layered elastic models, incorporating extra slip at depth, can reproduce coseismic displacements from a uniform elasticity dislocation model using the $M_w = 1.7 \times 10^{20}$ N m slip distribution, as reported by Reilinger *et al.* (2000). We also evaluated differences in stresses predicted by models of dislocations in layered and uniform elastic structures, when the models produce similar surface deformation. The hypothetical slip distributions were created by adding slip at 12–18 km and 12–24 km, respectively, to the coseismic slip distribution, as reported by Reilinger *et al.* (2000). The $M_w = 2.1 \times 10^{20}$ N m model gives Coulomb stresses comparable to the uniform elastic model at the Düzce hypocenter and at near-field points C and D on the Marmara Sea and Yalova faults, respectively (Fig. 1), but yields lower coseismic Coulomb stresses than the uniform elastic model in the far-field. This model fits surface displacements about as well as the uniform elastic model (WRSS = 7500), but the far-field displacements are consistently too small. The $M_w = 2.5 \times 10^{20}$ N m model gives greater coseismic Coulomb stresses at the Düzce hypocenter and at near-field reference points C and D than those estimated using a uniform elastic model (see subsequently). This model fits surface displacements somewhat better than our uniform elastic model (WRSS =

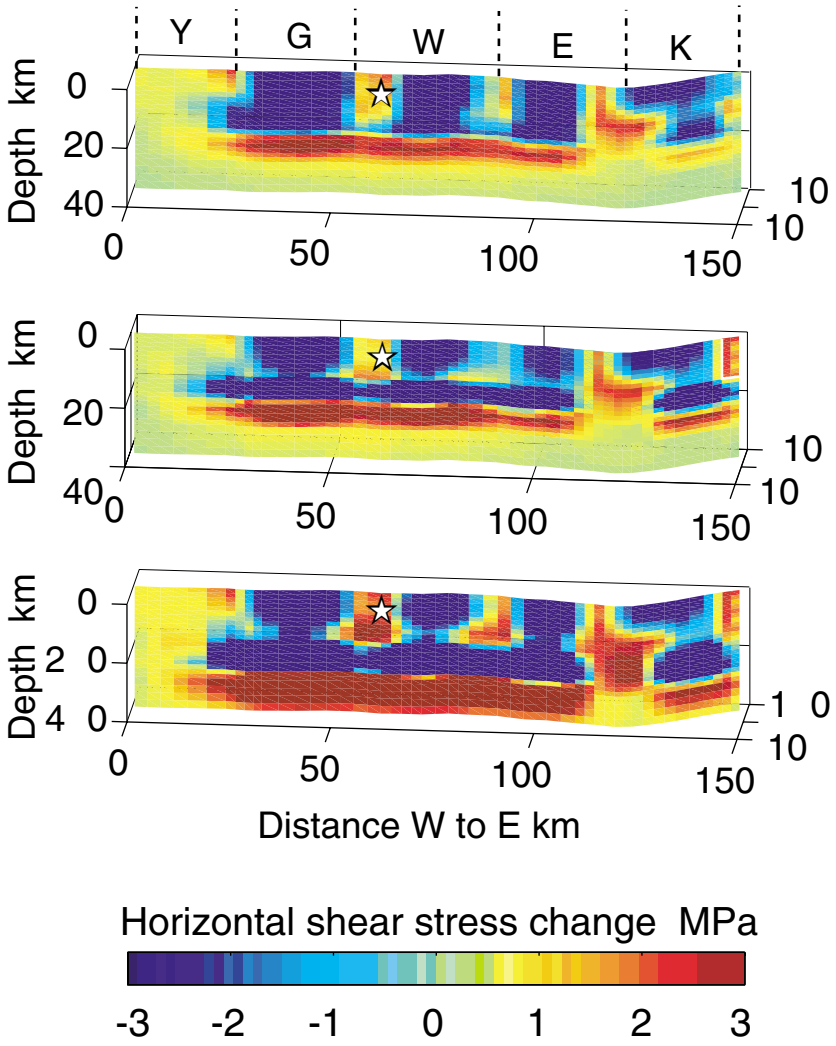

Figure 3. Coseismic shear stress on and below the İzmit rupture surface. Shear stress is resolved onto a plane tangent to the fault surface at each modeled fault node, and horizontal slip is assumed. The İzmit hypocenter is shown with a star. Y, G, W, E, and K are the Yalova, Golcuk, West Sapanca, East Sapanca, and Karadare segments, respectively. The top figure shows shear stresses for the uniform elastic model with G equal to 30 GPa and coseismic slip as reported by Reilinger *et al.* (2000). Given G (30 GPa) in the upper crust, M_w for this slip distribution is 1.7×10^{20} N m. The middle and bottom figures are for the layered elastic model (see text), using augmented slip distributions with M_w 2.1×10^{20} N m and 2.5×10^{20} N m, respectively. The top and bottom figures are from models that match coseismic surface displacements equally well, yet the modeled shear stresses are significantly different, especially below 10–15 km. In the lower crust near the hypocenter, for example, shear stresses in the top and bottom figures differ by a factor of 10.

3600, a 98% reduction relative to a model with zero displacement at all stations). Both the layered elastic models yield very large increases in shear stress on and below the İzmit rupture surface (by up to a factor of 3 and a factor of 10, respectively, in the lower crust below the hypocenter). We do not know exactly how the added deep slip required by the layered elastic models is distributed, so estimates of fault-zone stresses from these models are approximate.

Coseismic Coulomb Stress Changes on Neighboring Faults

Using our uniform elastic model, we estimated that the coseismic Coulomb stress increased by 0.14 MPa on a plane dipping 50° north at the Düzce hypocenter (dip of the Düzce rupture is from Ayhan *et al.,* 2001). In this location, the rupture surface experienced a right-lateral shear stress increase of 0.14 MPa and less than 0.01 MPa of compressional stress across the dipping fault surface. Our coseismic Coulomb stress estimate is consistent with the 0.1–0.2 MPa estimate of Parsons *et al.* (2001) and the 0.06–1.0 MPa estimate (for the entire Düzce rupture surface) of Hubert-Ferrari *et al.* (2001).

We also estimated coseismic Coulomb stresses at four points (Points A, B, C, and D) on the vertical strike-slip faults in the Marmara Sea (Fig. 1, points A–D). Points A, B, and C are located 160, 100, and 20 km west of the western end of the İzmit earthquake rupture, respectively, and point D is on the Yalova segment of the NAF, approximately 20 km from its western terminus. All these reference points (and the Düzce hypocenter) are at a depth of 9 km. At points A–D, we estimate coseismic Coulomb stresses of 0.003, 0.025, 0.20, and 0.48 MPa, respectively. For comparison, Parsons *et al.* (2001) estimated Coulomb stress increases of 0.05–0.5 MPa within about 40 km of the west end of the rupture, and Hubert-Ferrari *et al.* (2001) estimated Coulomb stress increases of 0.1 to 0.5 MPa within 25 km of the west end of the İzmit rupture.

Using our layered elastic model and the $M_w = 2.5 \times 10^{20}$ N m coseismic slip distribution, we estimated that the

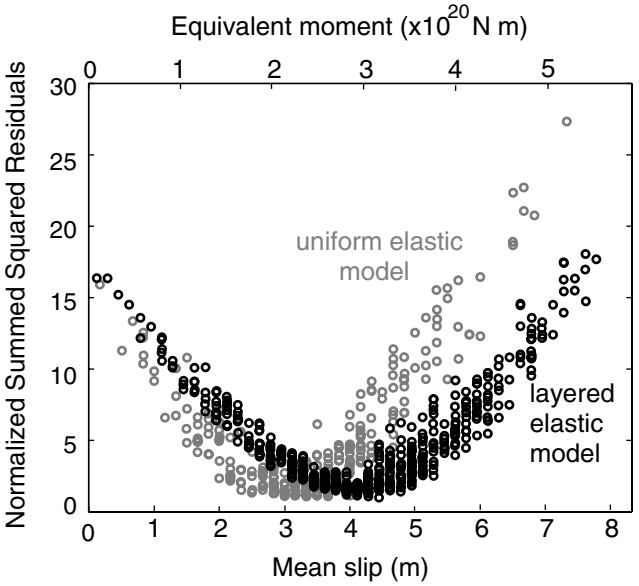

Figure 4. Monte Carlo coseismic slip inversions for uniform and layered elastic models. Each point represents a simulation with the mean slip shown. (Since there are three patches, several different slip distributions may yield the same mean slip.) Seismic moment is obtained from the mean slip assuming $G = 30$ GPa in the seismogenic zone. The summed squared residuals (SSRs) are normalized to the minimum SSR for the layered and elastic cases (each curve has a minimum of one).

coseismic Coulomb stress at the Düzce hypocenter is 0.24 MPa. In this case, the modeled Düzce rupture surface experienced a right-lateral shear stress increase of 0.19 MPa and about 0.1 MPa of tensional stress. At reference locations A–D, this model yields coseismic Coulomb stress increases of 0.002, 0.029, 0.22, and 0.76 MPa, respectively.

Afterslip Models

Creeping Viscous Shear Zone

For linear viscous shear zone models with uniform η/w, the best fit to time-dependent horizontal GPS displacements was obtained with $\eta/w = 1.0 \times 10^{13}$ Pa sec/m (e.g., $\eta = 1 \times 10^{16}$ Pa sec and $w = 1$ km). We also varied the depth below which viscous creep was permitted and found that a depth of 10 km overall worked better than 5 or 20 km.

For the best linear viscous shear zone model, the cumulative SSR over 28 stations (56 degrees of freedom) and eight 10-day time intervals, was 0.041 m^2 (this quantity is not weighted by the measurement errors). This represents a reduction of 69% relative to a model in which no postseismic displacement occurred. Figure 5 shows the sensitivity of SSR to the variation in η/w. Displacements measured at the continuous stations have small errors and contribute disproportionately to error-weighted measures of model misfit. Thus, the WRSS after 80 days is 290 for the best linear viscous

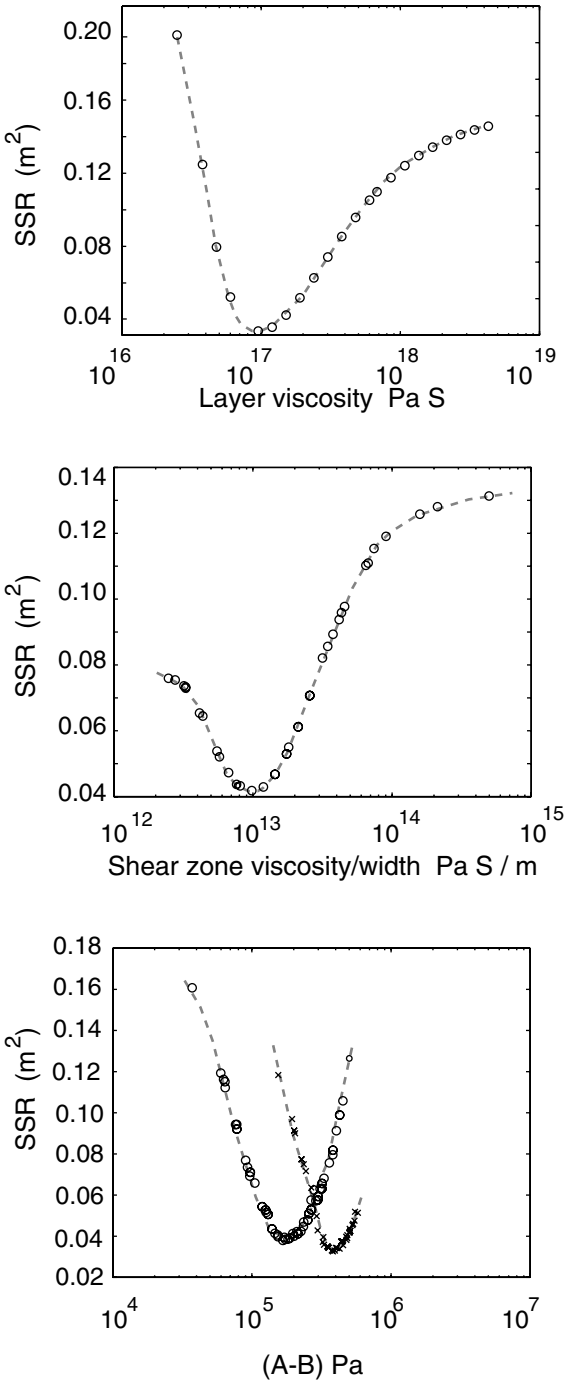

Figure 5. Sensitivity of cumulative summed squared residuals to changes in postseismic model parameters. Top, middle, and bottom figures are for the viscoelastic lower crust, linear viscous shear zone, and frictional afterslip models, respectively. In the bottom figure, results for models incorporating layered elastic structure are also shown (x). In all of the figures, the SSR is summed over eight 10-day time steps for all 28 GPS stations with three or more occupations between the İzmit and Düzce earthquakes. For comparison, a model with no surface displacement yields a SSR of 0.14.

shear zone creep model, but 90% of this is from the 10 continuous stations. Minimizing the WRSS and the SSR give the same η/w (1.0×10^{13} Pa sec/m).

Figure 6 and Table 1 show modeled and measured surface displacements 80 days after the İzmit earthquake (i.e., up to within 1 week of the Düzce earthquake), as reported by Ergintav *et al.* (2002). Our linear viscous shear zone model underpredicts postseismic displacements at GPS sites within 10 km of the rupture because no creep is modeled at depths shallower than 10 km. In the Marmara region, modeled displacements are too large and too fault parallel. Allowing slip only at depths exceeding 20 km resolves this problem but intensifies the misfit to near-field displacements to such a degree that the overall model fit to GPS data is compromised. (Conversely, allowing creep below 5 km depth reduces misfit at near-field stations, but significantly degrades the fit to displacements in the Marmara region.)

One way around the problem of insufficient near-field displacements might be to incorporate poroelastic rebound in the model (e.g., Peltzer *et al.,* 1998). We evaluate this possibility by modeling postseismic displacements caused by poroelastic rebound (Fig. 7) and determining whether scaling these displacements and adding them to the modeled displacements, shown in Figure 6, could reduce the misfit to GPS data in the near field. Figure 7 shows that near-fault displacements caused by poroelastic rebound are mainly fault normal and are largest near the ends of the rupture. This suggests that the additional, fault-parallel motion required at near-field stations such as SMAS, MURT, and SISL cannot be supplied by poroelastic rebound.

South of the İzmit rupture, modeled displacements are more fault-parallel than GPS observations (Fig. 6, stations MEKE, IUCK, IGAZ, and AGUZ). This is true for all of the models presented in this article: the contribution to the cumulative SSR from these four stations is 0.011, or 20% of the total SSR for all the 28 stations. Triggered creep on the Iznik Valley fault and possibly the Mudurnu Valley fault, detected on InSAR interferograms (Wright *et al.,* 2001; Feigl *et al.,* 2002), may have occurred postseismically and thus may cause some of the model misfit in this region.

Figure 8 shows afterslip on and below the İzmit rupture at several time intervals between the İzmit and Düzce events.

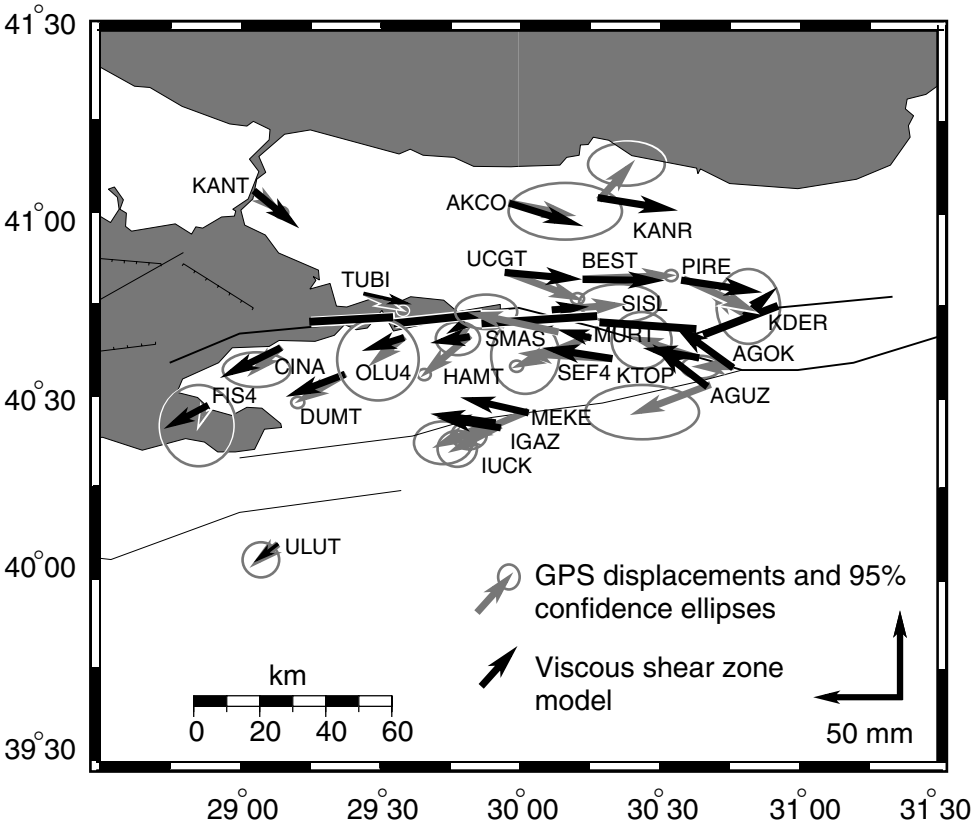

Figure 6. Modeled and measured (or interpolated) GPS station displacements after 80 days for the linear viscous shear zone model. Note the small modeled displacements in the near field (SMAS, SISL, and GLCK) and large modeled displacements in the Marmara region (OLU4, CINA, DUMT, FIS4, and KANT). Model fit to the data is poor south of the rupture (IGAZ, MEKE, IUCK, and AGUZ). This may be because of triggered slip on the Iznik and Mudurnu Valley faults (Wright *et al.,* 2000), or a very large amount of slip at depth on the Karadare segment (Reilinger *et al.,* 2000; Bürgmann *et al.,* 2002), which none of our dynamic afterslip models can produce.

Table 1
Modeled and Measured Postseismic Displacements After 80 Days

	East	Sigma	FS	LVC	VELC	North	Sigma	FS	LVC	VELC	Up	Sigma	FS	VLC	VELC
Continuous Stations															
ANKR	−6	1.6	−1.6	−3.1	−2	2	1	0.9	1.9	0.6	−3.5	2.5	0.1	0.3	−0.5
MURT	−44	1.5	−24.7	14.3	−20	−18	1.2	−4.8	2.8	8.7	−7.1	4.7	6.2	−3.1	−1.8
BEST	53	1.6	38.9	45.2	40.8	2	1.1	−0.3	−2.5	6.1	−20.8	4.1	−1.4	−2	2.7
UCGT	43	1.6	22	40.1	45.5	−16	1.1	−5.2	−5.3	0	−36.7	3.8	−0.5	−2.5	−2.6
HAMT	−26	2	−27.7	−18.9	−22	−22	1.5	−33.8	−4.6	−5.9	−6.1	4.5	6.3	4.9	1.3
TUBI	21	1.5	13.2	24.9	21.1	−9	1	−11.8	−6.5	−22.3	−16.5	3.6	−8.2	−3	3.9
KANT	13	1.4	13.2	22.9	29.6	−10	1	−11.4	−19	−15.6	−6.7	3.6	−1.9	−4.4	−1.4
DUMT	−26	1.3	−21.5	−32.2	−29.6	−15	1	−14.4	−11.2	−20.6	−8	3.1	7.3	7.8	4.7
MERT	−2	2	1.4	3.2	3.4	−1	1.4	−1.2	−2.5	0.8	−6.9	4.2	0	0.1	−0.9
ULUT	−12	7.4	−8.9	−13.7	−19.8	−10	6.3	−8.1	−11.2	−22.6	−15.2	13.3	−0.2	0.4	12
Campaign-mode Stations															
AGOK	−19	7.7	−27.6	−35.2	−25	0	4.6	27.8	21.8	8.4	−7	22	−18	−19.7	−5
IUCK	−27	7.4	−27.4	−37.6	−44.9	−14	7	4.5	3.8	−3.5	−13.7	25	−4.5	−3.1	2
IGAZ	−32	8.6	−27.7	−38.4	−46.5	−14	11	2.8	3	−4.8	−28.2	22	−4.2	−2.8	2.8
KTOP	−38	11	−20.3	−32.3	−20.9	12	11	27.8	6	12.9	−21.2	130	−8.4	−7	−2.5
PIRE	40	11	35.6	42.1	37.2	−18	14	−8.1	−7.3	15.3	6.9	18	−6.5	−7.7	1.2
SEF4	−53	9.2	−23	−36.4	−36	3	13	1.2	5.8	13.4	−19.8	46	−9.9	−6.5	−2.6
KANR	18	9.2	28.6	41.4	43.2	20	7	−3.2	−7.4	11.8	0.3	33	−0.3	−2.7	8.5
MEKE	−38	6.9	−33.7	−41.3	−48.7	−16	5.5	11.5	6.9	3.3	−9	20	−5.8	−4.7	−2.4
AKCO	36	22	26.5	39	45.1	−7	9.7	−13.6	−11.2	−3.3	19	65	−3.5	−4.3	−3.2
GLCK	−5	6.7	−9	−6	−7.2	−13	4.8	−36	−3.8	−6.4	1.7	20	4.7	4.4	0
OLU4	−17	18	−16.9	−21	−16.5	−14	18	−11.4	−5.9	−23	−37.6	140	7	3.4	−4.3
SISL	40	11	49.4	16.2	11.8	3	8	15.7	0.4	3.8	−9.4	26	5.2	3.4	−1.3
CINA	−16	11	−14.9	−28.8	−19	−14	6.5	−10.3	−14.2	−13.2	70.3	222	5.2	9.8	5.3
SMAS	−51	11	−45.7	−10.1	−12.8	11	7.3	10.2	0.9	4.6	−38.7	36	5.1	0.9	−2.5
FIS4	−4	13	−9.4	−19.4	−20.1	−10	20	−6.3	−13.1	−4.7	−25	71	0.6	3.3	8.3
MADT	2	1.4	−0.5	−1.2	−0.5	2	0.8	0.6	−1.2	0.8	−4.7	3.6	0	0	0.1
AGUZ	−45	22	−25.7	−31.7	−34.7	−17	13	30.7	23.3	12.3	−16	46	−14.8	−16.7	−7.5
KDER	−22	86	22.9	16.8	6.8	13	36	10.1	11.8	10.8	−11.7	170	10.2	22.3	−2.9

FS, frictional afterslip; LVC, linear viscous fault zone creep; VELC, viscoelastic lower crust. At campaign-mode stations, displacements at 80 days are interpolated using functions as reported by Ergintav *et al.* (2002).

Since the creep rate is proportional to $d\tau$, significant slip occurs in areas of positive coseismic shear stress off the fault ends and on and below the rupture surface. Slip is concentrated below the hypocenter and on the western Karadare fault segment and occurs at greater depths as time progresses, consistent with postseismic slip inversions (Bürgmann *et al.,* 2002). However, unlike the inversions, this model yields significant afterslip west of the coseismic rupture and no slip at depths of less than 10 km on the İzmit rupture surface.

Velocity-Strengthening Frictional Slip

For our frictional afterslip models with uniform values of A-B, the best fit to time-dependent GPS data was obtained using $(A\text{-}B) = 0.19$ MPa (0.43 MPa for the layered elastic model). Figure 5 illustrates how sensitive the SSR between the modeled and GPS surface displacements is to this parameter. The SSR, summed over 28 stations (56 degrees of freedom) and eight 10-day time intervals, is 0.040 m^2 (0.036 m^2 for the layered elastic model). The WRSS between the modeled and measured displacements after 80 days is 190.

The fit of modeled site displacements to GPS displacements in the very near field is superior to that for the viscous shear zone model because of near-surface creep (Fig. 9 and Table 1). At continuous stations HAMT and MURT, the frictional afterslip model yields fault-normal displacements comparable to observations, which are due to end-effects from shallow, high-afterslip patches on the fault. Displacements at SISL and SMAS are also modeled well because of shallow afterslip. For stations in the Marmara Sea region (HAMT, KANT, TUBI, OLU4, CINA, DUMT, FIS4, and ULUT), the SSR is 0.0019 m^2, compared with 0.0044 m^2 for the viscous shear zone model. Modeled displacements beyond the west end of the İzmit rupture are smaller and more fault normal than estimated by the viscous shear zone model, resulting in a better fit to the data in the Marmara region. Displacements in this region are smaller and more fault-normal because there is less slip at depth beyond the end of the coseismic rupture (see Fig. 8). This is because afterslip is proportional to $e^{d\tau}$ (rather than to $d\tau$) and is thus more localized to the most highly stressed regions than it is for the viscous shear zone model. Afterslip is concentrated at and below the hypocenter and the western Karadare segment, which is more consistent with slip inversions (Reilinger *et al.,* 2000; Bürgmann *et al.,* 2002).

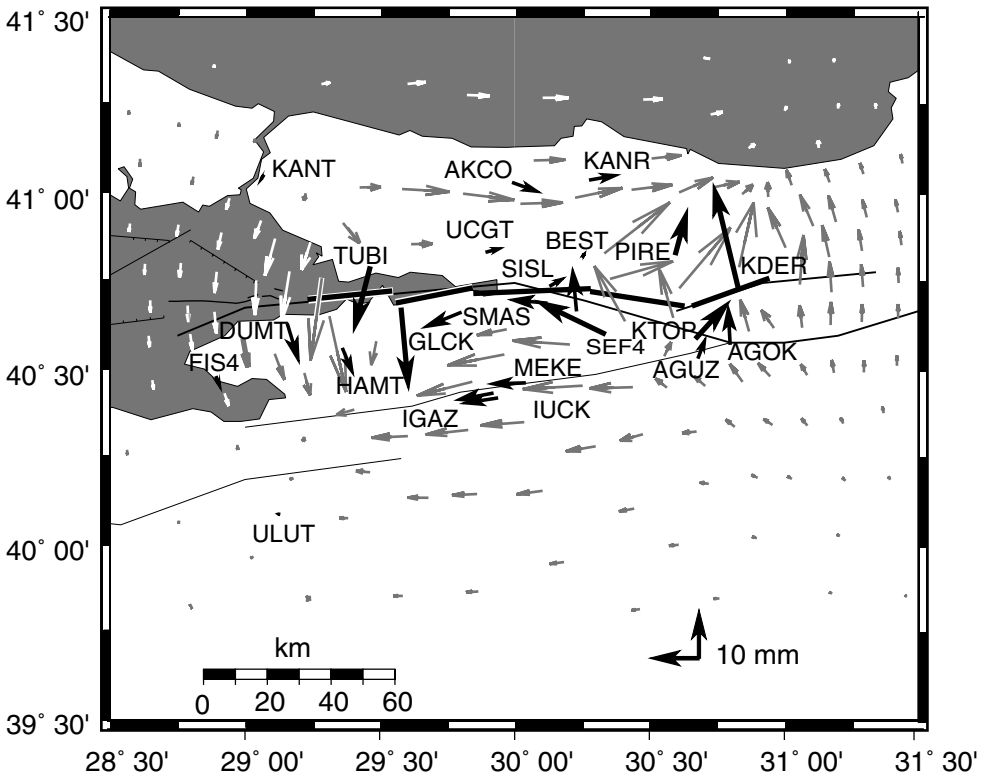

Figure 7. Horizontal displacements caused by poroelastic rebound. Displacements are calculated at GPS sites (dark arrows) and at other locations (light arrows), which are shown to give some sense of the overall displacement pattern. The largest displacements caused by poroelastic rebound are near the fault ends (or the ends of high slip patches) and are fault-normal. Displacements are fault-parallel at near-field stations SMAS and SISL but are small. Scaling these vectors and adding them to the vectors shown in Figure 6 will not improve the fit of the linear viscous shear zone model vectors to GPS displacements.

For the models in which the value of (A-B) increases linearly below 15 km depth, the best results are obtained when the upper crustal (A-B) is 0.10 MPa (0.17 MPa for the layered elastic model). For these models, far-field displacements are lower than for models with uniform A-B values due to inhibited slip at depth. This difference raises the cumulative SSR in the Marmara region by a factor of 4 and increases the total SSR to 0.076 (0.065 for the layered elastic model). Thus, our modeling favors a fault that is weakly velocity-strengthening below, as well as within, the upper crust.

Viscoelastic Lower Crust Model

Relaxation of a linear viscoelastic layer at 24–30 km depth, with a viscosity of 5.0×10^{16} Pa sec, reproduces the surface displacements between the two earthquakes about as well as the frictional afterslip model (Fig. 10 and Table 1). The cumulative SSR is 0.036 m^2, representing a reduction of 72% relative to a model with no postseismic displacement. Similar (but not identical) horizontal displacements are obtained with alternate models in which η/layer thickness is identical, as long as the top of the viscoelastic layer is at a depth of about 24 km. The sensitivity of the cumulative SSR to changes in viscosity for a 6-km-thick, lower crustal layer is shown in Figure 5.

The WRSS for 80-day displacements is greater for this model than for the other two models (390 versus 290 for the viscous shear zone model and 190 for the frictional afterslip model). This is because this model fits displacements at stations with large measurement errors better than it fits displacements at continuous stations and campaign-mode stations with relatively small measurement errors. As with the viscous shear zone model, near-field postseismic displacements are underestimated, and poroelastic rebound in the uppermost crust cannot make up the difference between modeled and observed near-field displacements.

The required lower crustal viscosity for our best linearly viscous lower crust model (1.0×10^{17} Pa sec) is consistent with volatile-rich, quartz-bearing rocks, deforming at high temperatures (450–600°C for wet quartzites, Jaoul *et al.,* 1984; Wang *et al.,* 1994). Our linear viscous lower crust model could also represent weakly nonlinear deformation (such as that of wet Westerly granite, with $n < 2$, Hansen and Carter, 1983), which would be indistinguishable from

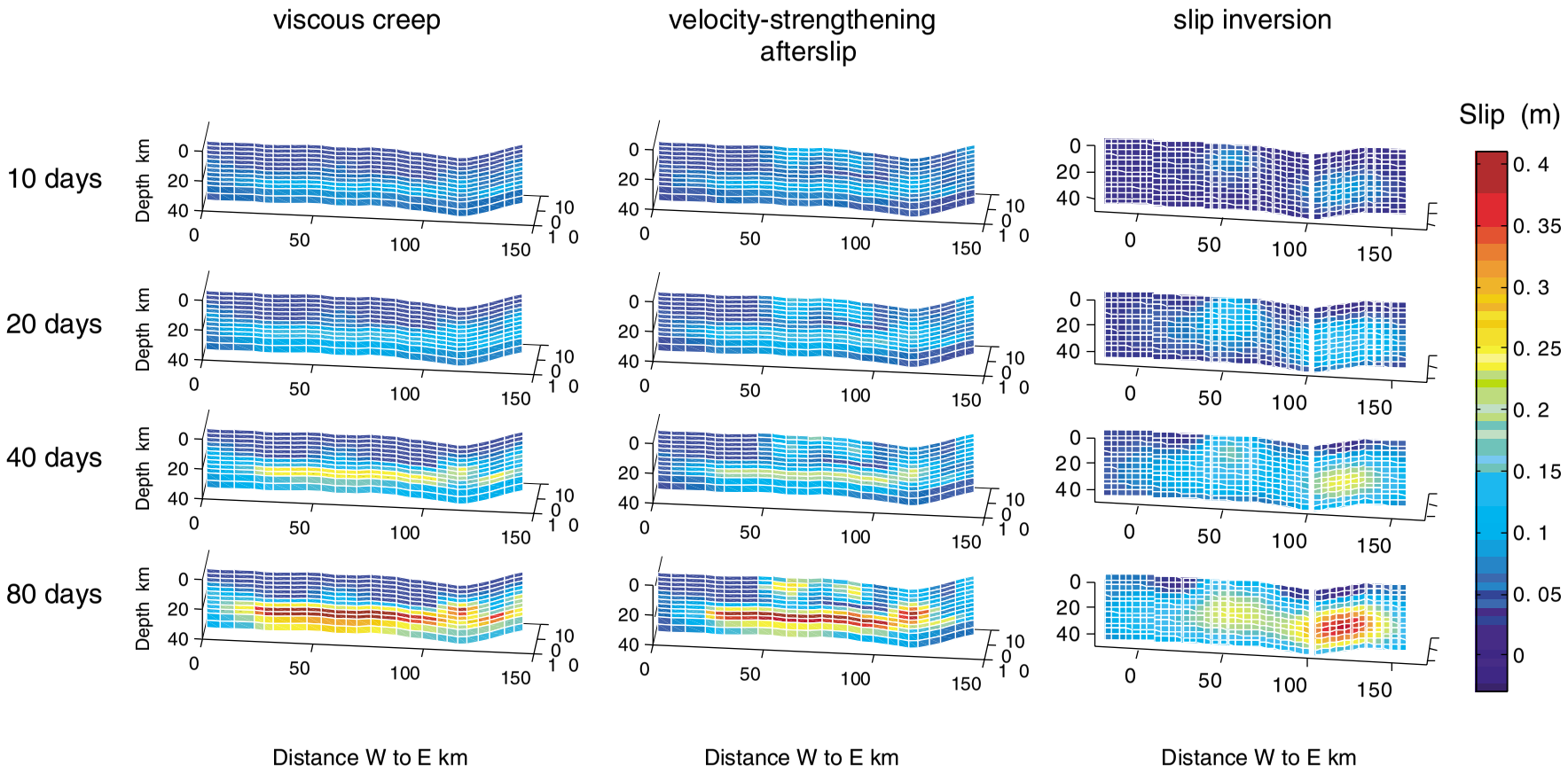

Figure 8. Total afterslip on and below the İzmit rupture surface 10, 20, 40, and 80 days after the earthquake. The first and second columns show modeled slip from our best linear viscous shear zone creep and frictional afterslip models. The third column shows the slip distribution necessary to match coseismic surface displacements (Bürgmann *et al.,* 2002). Both our models reproduce high afterslip at the hypocenter and on the Karadare segment, which is distributed over increasing average depths with time. Our frictional afterslip model also reproduces the lack of afterslip below the Yalova (westernmost) segment. Our models do not reproduce the high magnitude of afterslip on the Karadare segment. Either a process we cannot model is occurring, or the slip inversions are influenced heavily by GPS data from stations that may be affected by triggered afterslip on nearby faults (i.e., MEKE, IUCK, IGAZ, and AGUZ).

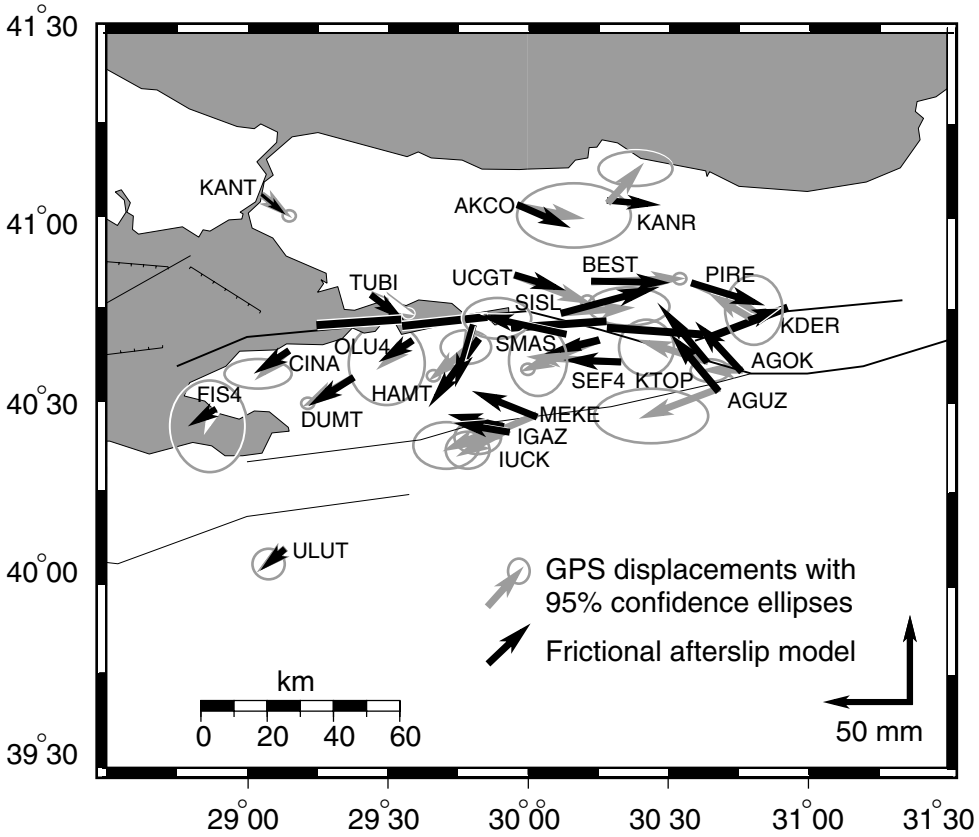

Figure 9. Modeled and measured (or interpolated) GPS station displacements after 80 days for the velocity-strengthening frictional afterslip model. This model does the best job of fitting GPS data at sites in the Marmara region (because afterslip on the Yalova segment is suppressed) and at sites close to the earthquake rupture (because shallow afterslip is permitted). This model also reproduces displacements at sites with the smallest measurement errors (such as continuous stations) better than competing models.

linearly viscoelastic deformation if the pre-earthquake differential stress exceeded about 10 MPa in the lower crust. Given the surface heat flow of 70–80 mW/m^2 along the western NAFZ, and other thermal parameters as reported by Mueller *et al.* (1997), temperatures exceeding 450°–500°C could be attained at depths exceeding about 20 km. However, a weak viscoelastic layer would probably manifest itself at the surface by widening the plate boundary shear zone at the surface (Roy and Royden, 2000). This is not consistent with the relatively simple and narrow geometry of the NAF system in this part of Turkey. In addition, the viscosity required by our model is significantly lower than most viscosity estimates for weak, continental lower crust (e.g., $\sim 10^{18} - 10^{19}$ Pa sec, Li and Rice, 1987; Kruse *et al.,* 1991).

Another major problem with the linearly viscoelastic lower crust model is that it does not adequately reproduce the decay in early postseismic surface velocities with time. Our model that best fits surface displacements between the İzmit and Düzce earthquakes significantly overestimates station displacements 300 days after the earthquake (Ergintav *et al.,* 2002), particularly in the far-field.

We can contrive a nonlinearly viscous lower crust model to produce decaying surface velocities that are more consistent with GPS observations. A successful nonlinear lower crust model would have to have an effective viscosity that (1) was initially about 1×10^{17} Pa sec in the vicinity of the earthquake (comparable to our linearly viscoelastic lower crust result), and (2) increased to at least $10^{18} - 10^{19}$ Pa sec after lower crustal stresses returned to pre-earthquake levels. Effective viscosity of a nonlinear material drops with increased stress as shown by equation (3).

$$\frac{\eta}{\eta_0} = \left(\frac{\sigma_0}{\mathrm{d}\sigma + \sigma_0} \right)^{n-1}, \tag{3}$$

$\mathrm{d}\sigma$ is the coseismic differential stress increase, σ_0 is the pre-earthquake differential stress, n is the stress exponent, η_0 is the pre-earthquake effective viscosity of the lower crust, and η is the effective viscosity just after the earthquake. Given a coseismic stress change in the near-field lower crust of 5 MPa and $n = 3$, pre-earthquake stress (σ_0) would have to

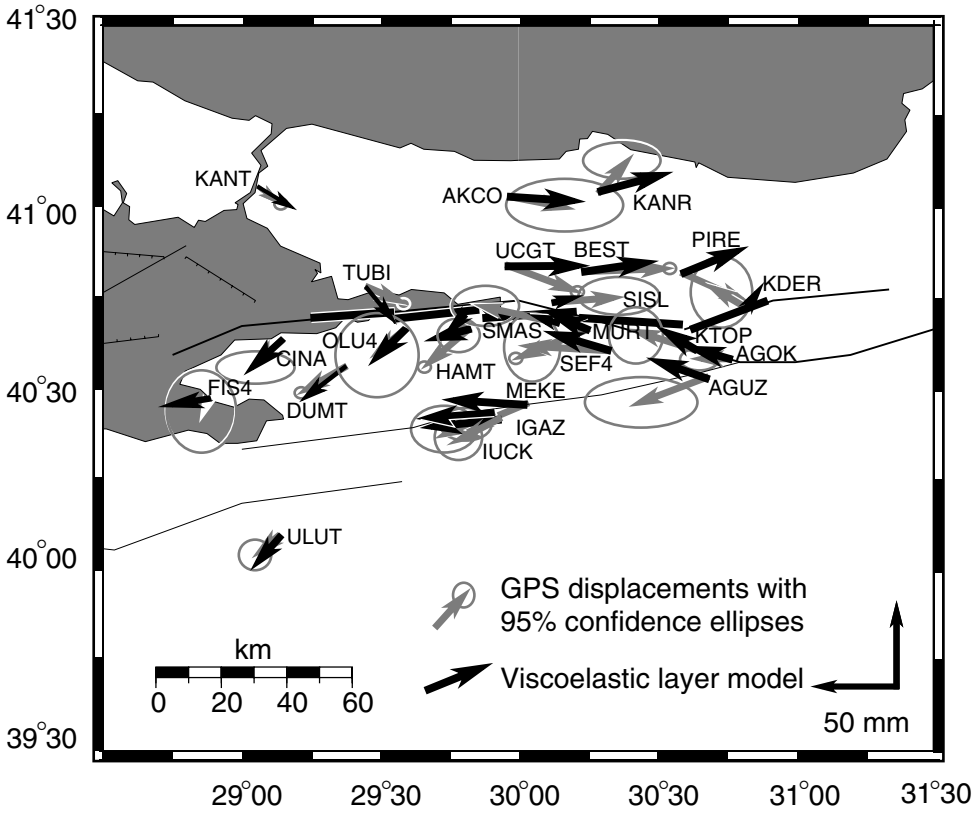

Figure 10. Modeled and measured (or interpolated) GPS station displacements after 80 days for the linear viscoelastic layer relaxation model. This model systematically overestimates far-field displacements and underestimates displacements close to the rupture trace, but because of smaller residuals at MEKE, IGAZ, IUCK, and AGOK, the SSR is comparable to that of the frictional afterslip model (though the weighted residual sum of squares [WRSS] is much greater).

be 0.5–2 MPa to drop effective viscosity by a factor of 10–100, as required by equations (1) and (2). Experimentally derived nonlinear flow laws for typical quartzofeldspathic rocks (a summary has been given by Carter and Tsenn, 1987) show that several rock types could produce such behavior at temperatures exceeding 400°C, but the strain rates associated with the required pre-earthquake stresses would have to be of the order of 10^{-19}/sec. These values are several orders of magnitude lower than strain rates thought to be typical of deforming continental crust at plate boundaries ($\sim 10^{-14} - 10^{-15}$/sec). Furthermore, the required pre-earthquake stress is so low that linearly viscous diffusion creep, rather than nonlinear power law creep, would likely be the dominant process (e.g., Tsenn and Carter, 1987). For these reasons, nonlinear viscous deformation of the lower crust is not likely the main cause of accelerated, early post-İzmit earthquake deformation.

Postseismic Stresses at the Düzce Hypocenter

Using our best frictional afterslip model, we estimated that Coulomb stress at the Düzce hypocenter (for horizontal right-lateral slip on a plane dipping 50° north) increased by 0.1 MPa during the 87 days between the İzmit and Düzce earthquakes (Figs. 11 and 12). Our linear viscous shear zone model indicates that Coulomb stress increased by 0.12 MPa during this interval. These stress estimates have high uncertainties because both the models perform poorly at fitting available surface displacement data from the Düzce region prior to the 12 November earthquake.

Postseismic Coulomb stress estimates from the frictional afterslip model are highly sensitive to the depth interval over which afterslip is permitted beyond the east end of the İzmit rupture. Our default assumption is that beyond the ends of the coseismic rupture, frictional afterslip can occur below a depth of 15 km. If no afterslip is permitted at any depth east of the İzmit rupture, the total postseismic Coulomb stress change at Düzce is 0.02 MPa. If afterslip is permitted at all depths (i.e., the velocity-strengthening parameters used for the coseismic rupture are also used beyond the rupture boundaries), the total postseismic Coulomb stress change at the Düzce hypocenter before the 12 November earthquake is about 0.13 MPa. (In this case, the Coulomb stress actually starts to decline before the Düzce earthquake, as stress is released by creep at the hypocenter.) Neither of these possibilities may be ruled out by GPS data from east

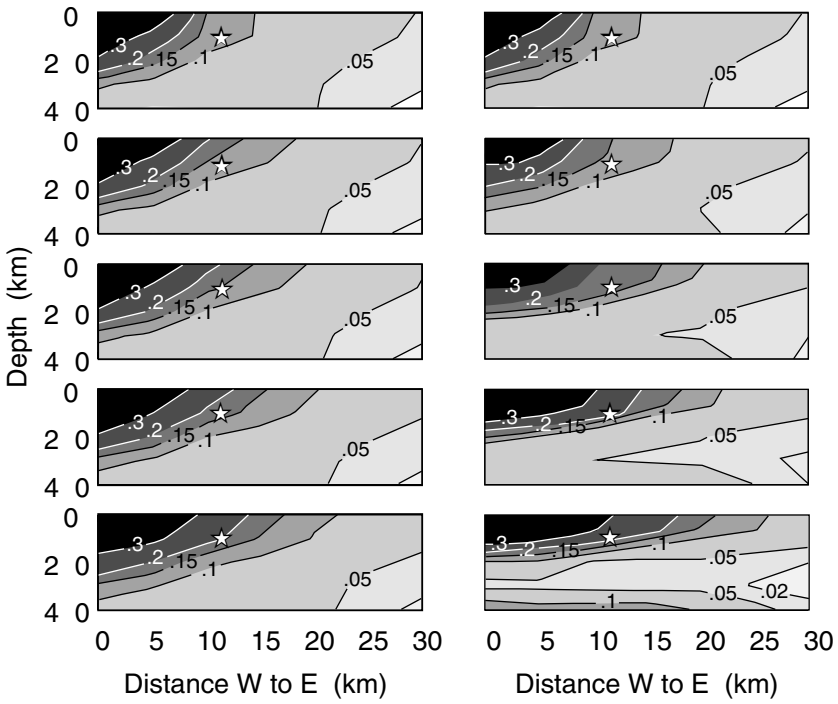

Figure 11. Coulomb stress (MPa) at the Düzce hypocenter 0, 10, 20, 40, and 80 days after the İzmit earthquake, from models incorporating frictional afterslip (left) and linear viscous shear zone creep (right). These stress calculations are for horizontal slip on a surface dipping 50° N at the Düzce hypocenter coordinates. The linear viscous creep model transfers more stress to the upper crust than the frictional afterslip model, particularly beyond the Düzce hypocenter, because more afterslip is modeled at depth beyond the east end of the İzmit rupture. The spatial variation in Coulomb stress on this surface illustrates that error ranges for the modeled stresses (Fig. 12) are large, even when the poor resolution of GPS surface displacement data in this area is not taken into account.

of the İzmit rupture; there are too few reliable measurements to adequately constrain the distribution of afterslip in this area.

Postseismic Stresses on Marmara Sea Faults: First 300 Days

To evaluate how models that fit GPS data collected prior to the Düzce earthquake perform over a longer time interval, we forward model displacements for 300 days after the İzmit earthquake and compared them with GPS data (reported by Ergintav *et al.,* 2002). The displacement data are corrected for the Düzce earthquake coseismic displacements and for secular deformation. We focus our comparison on sites in the Marmara region, where Düzce earthquake postseismic effects are limited. Figure 13 illustrates that our velocity-strengthening frictional afterslip model fits time-dependent, horizontal surface displacements better than the competing models at the five continuous GPS stations of the Marmara area.

Unlike the horizontal data, vertical displacement data are not well fit by any of the models. This may be because of shallow crustal processes (such as groundwater pumping) that are not modeled. Furthermore, errors in vertical displacements may significantly exceed the formal one-sigma errors shown in Table 1 (as the presence of large, spatially correlated anomalies in the vertical displacement data would suggest).

Modeled Coulomb stresses at Marmara Sea points A, B, C, and D during the first 300 days after the İzmit earthquake are shown in Figure 14. At all four points, we estimate Coulomb stresses for right-lateral, horizontal slip on vertical surfaces at 9 km depth. The frictional afterslip model, which fits the GPS data better than the linear viscous shear zone and lower crust models in this area, indicates that postseismic Coulomb stress change during the 300 days after the İzmit earthquake was about 15%–25% of the coseismic Coulomb stress magnitude at these points. The postseismic Coulomb stress magnitude relative to the coseismic Coulomb stress increases with distance from the fault, but both values are less than 0.01 MPa beyond about 120 km from the rupture.

Secular Coulomb stressing rates of 0.01 MPa/yr (Straub *et al.,* 1997; Hubert-Ferrari *et al.,* 2001, southern Marmara region) to 0.04 MPa/yr (Hubert-Ferrari *et al.,* 2001) are inferred for the major NAFZ faults in the Marmara Sea. Only at points C and D in the near field does the frictional afterslip model predict postseismic stressing rates comparable to or greater than the minimum inferred secular stressing rate, and the post-İzmit Coulomb stressing rate at points C and D falls far below the minimum secular rate by 100–200 days after the earthquake. Beyond about 100 km from the west end of the İzmit rupture (point B), the frictional afterslip model suggests that the postseismic Coulomb stressing rate never exceeds the minimum secular stressing rate.

The linear viscous shear zone creep and viscoelastic lower crust models predict far greater stressing rates on the Marmara Sea faults than the frictional afterslip model. In the near field, the viscous shear zone model yields the largest Coulomb stresses, whereas in the far-field, the viscoelastic lower crust model predicts greater Coulomb stresses. After 300 days, postseismic stresses estimated by these models are

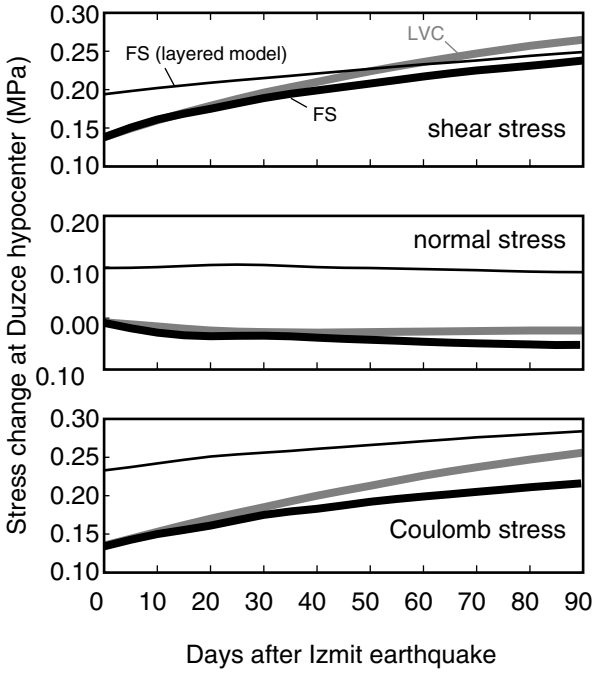

Figure 12. Coseismic and postseismic stresses at the Düzce hypocenter between the İzmit and Düzce earthquakes. FS, velocity-strengthening frictional afterslip model (uniform and layered elastic cases are both shown); LVC, linear viscous shear zone creep model. Shear stress changes are responsible for most of the Coulomb stress increase for both afterslip models when a uniform elastic structure is modeled. For the elastically layered model (with our M_w 2.5 $\times$ 10^{20} N m slip distribution) the coseismic Coulomb stress is greater, and tension across the Düzce fault surface contributes a significant component to the Coulomb stress.

up to an order of magnitude greater than those from the frictional afterslip model. The linear viscous shear zone and viscoelastic lower crust models also predict postseismic stressing rates in excess of the secular rate for at least 300 days after the İzmit earthquake at all reference locations but A (160 km from the rupture). The large differences between models in estimated Marmara fault stresses and stressing rates are important because these models produce roughly comparable postseismic velocities at the Marmara region GPS sites (Fig. 13).

Discussion

We have modeled time-dependent surface deformation between the İzmit and Düzce earthquakes, assuming either linear viscous creep or velocity-strengthening frictional afterslip on and below the İzmit rupture and contiguous surfaces to the east and west. We favor velocity-strengthening frictional afterslip over linearly viscous shear zone creep or viscoelastic lower crust relaxation to explain early postseismic deformation following the İzmit earthquake. This finding does not rule out the possibility that another form of nonlinearly stress-dependent shear zone creep could also be responsible for the early postseismic deformation. Such creep would have to occur rapidly on the İzmit rupture (but not beyond its ends) and in the midcrust, at temperatures of less than 400°–500°C.

Our frictional afterslip model is consistent with geologically constrained, conceptual models of crustal-scale continental fault zones, which involve frictional slip in the upper to middle crust, and viscous creep on a widening shear zone at greater depths (e.g., Sibson, 1983; Hanmer, 1988). Viscous creep may be underway at depth along the NAFZ and could contribute to longer term (slowly decaying) postseismic deformation of the crust around the İzmit rupture. We suggest, however, that linear viscous creep deep on the NAFZ did not begin to contribute significantly to the postseismic deformation during the first 300 days after the earthquake: if it had, more afterslip (and larger fault-parallel displacements) would have been observed at the Marmara region GPS stations. (Given sparse GPS coverage east of the İzmit rupture, and possible triggered slip and Düzce postseismic deformation in this area, we do not feel justified in speculating on patterns of [and mechanisms for] postseismic slip east of the İzmit rupture.)

Although the cumulative SSRs over the first 80 days are comparable for all the three models, the frictional afterslip model fits GPS displacement data better in the near-field and the Marmara Sea region, and at sites where measurement errors are small (such as the continuous stations). The frictional afterslip model also fits displacements during the first 300 days after the İzmit earthquake better than the viscous shear zone model or the viscoelastic lower crust model (Fig. 13). In the region where our frictional afterslip model fits the data most poorly (south of the rupture, at stations IGAZ, AGUZ, MEKE, and IUCK), triggered creep may have distorted the ground surface, causing localized misfit between our models and the data (Feigl *et al.,* 2001; Wright *et al.,* 2001). As reported in our companion article (Bürgmann *et al.,* 2002), the slip inversions assume that data from IGAZ, AGUZ, MEKE and IUCK are reliable, resulting in a solution with very high slip on the western Karadare segment. If this assumption is correct, and motion of these stations does reflect postseismic processes associated with the İzmit fault, we do not adequately model postseismic deformation east of the rupture, and our estimates of Coulomb stress at the Düzce hypocenter may be too low. High slip on the Karadare segment would have a small to negligible effect on our postseismic Coulomb stress estimates for faults in the Marmara Sea region.

Another feature of post-İzmit GPS surface displacement data that is more consistent with a frictional afterslip model than with the competing models presented in this study, is a very rapidly decaying velocity-transient ($t_c < 12$ hr) at continuous GPS stations TUBI and DUMT (T. A. Herring, 1999, personal comm.). This transient appears to have a magnitude that is less than half that of the $t_c = \sim 60$-day transient but

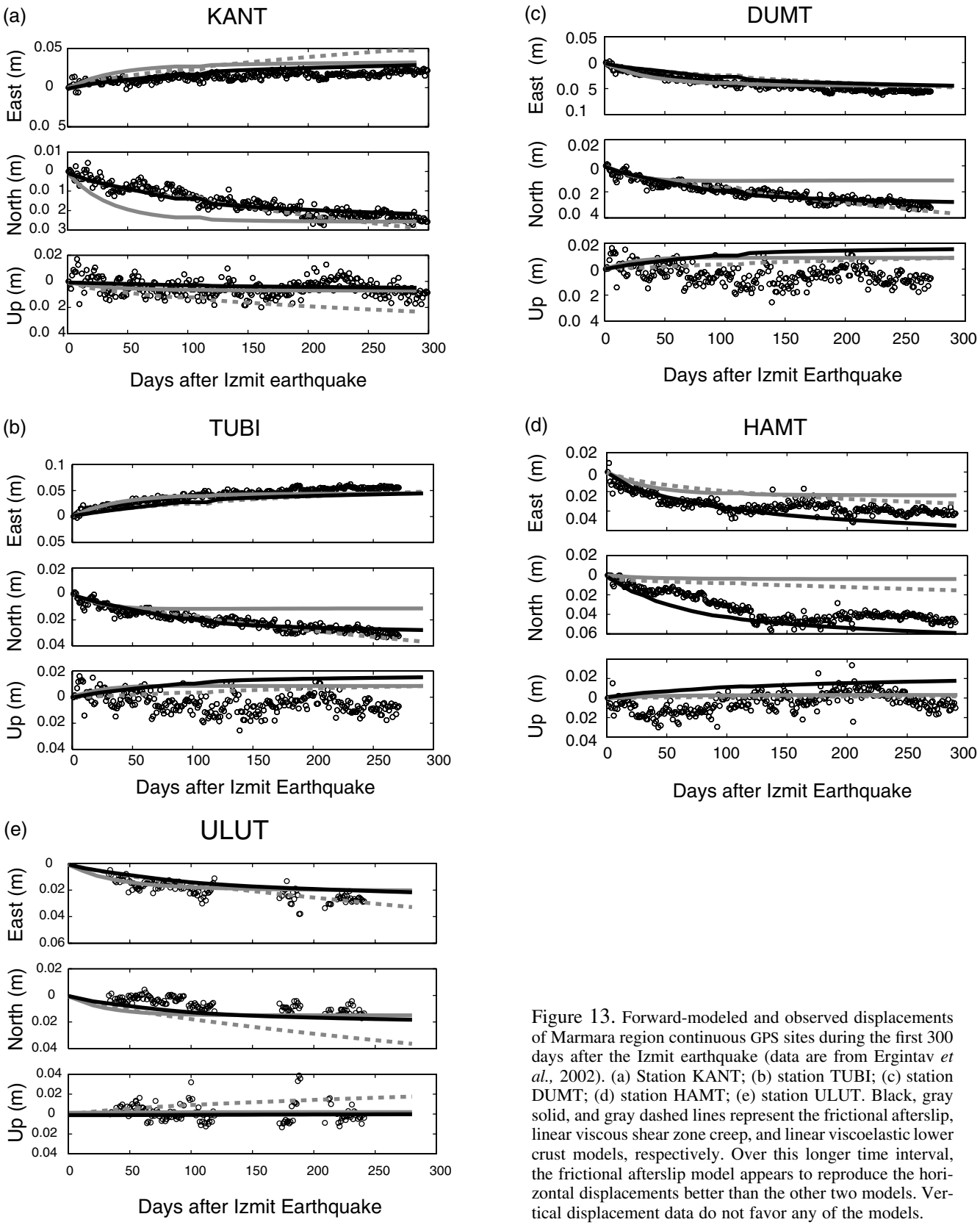

Figure 13. Forward-modeled and observed displacements of Marmara region continuous GPS sites during the first 300 days after the Izmit earthquake (data are from Ergintav *et al.,* 2002). (a) Station KANT; (b) station TUBI; (c) station DUMT; (d) station HAMT; (e) station ULUT. Black, gray solid, and gray dashed lines represent the frictional afterslip, linear viscous shear zone creep, and linear viscoelastic lower crust models, respectively. Over this longer time interval, the frictional afterslip model appears to reproduce the horizontal displacements better than the other two models. Vertical displacement data do not favor any of the models.

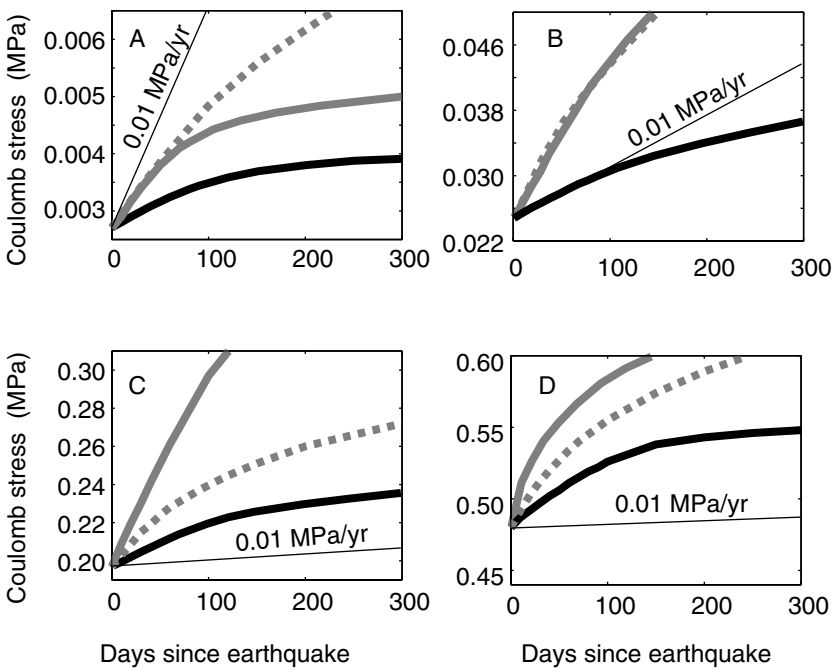

Figure 14. Modeled coseismic and postseismic Coulomb stresses at reference points A, B, C, and D (shown in Fig. 1) during the first 300 days after the İzmit earthquake. The Coulomb stress is for horizontal, dextral slip on vertical E–W-oriented surfaces and is calculated at 9 km depth. Black, gray solid, and gray dashed lines represent the frictional afterslip, linear viscous shear zone creep, and viscoelastic lower crust models, respectively. The frictional afterslip model consistently yields less postseismic stress transfer than the other two models. The viscoelastic lower crust model yields the greatest Coulomb stress changes in the far-field, whereas the viscous fault-zone creep yields the largest Coulomb stress changes in the near field. Figure 13 illustrates that modest differences in Marmara region ground surface displacements accompany these diverse postseismic stressing histories.

is too large to have been produced by aftershocks. Such rapidly decaying surface strain immediately after the earthquake is consistent with velocity-strengthening frictional afterslip because the slip rate is proportional to $e^{d\tau}$ (rather than to $d\tau$). This can lead to a very rapid initial slip on localized, highly stressed parts of the fault surface. Rapidly decaying postseismic velocity transients with t_c less than 3 days are documented in strain meter and continuous GPS data following earthquakes in many parts of the world (e.g., Wyatt *et al.,* 1994; Heki *et al.,* 1997; Bechor *et al.,* 2001; Bürgmann *et al.,* 2001). In the case of earthquakes on dipping faults, this deformation has been attributed to aseismic slip (mechanism unspecified) or to velocity-strengthening frictional afterslip. Since these very rapidly decaying velocity transients seem to follow earthquakes in varied tectonic settings, a single process that is common to diverse crustal environments, such as frictional afterslip, seems the most plausible cause. It is reasonable to suppose that such afterslip can continue at increasingly modest rates during the weeks following an earthquake, perhaps on fault patches that were more moderately stressed than those responsible for the transient of t_c less than 12 hr.

Our best estimate of velocity-strengthening parameter (A-B) is smaller than expected, given the accepted values of (a-b) and σ_n' in velocity-strengthening parts of the midcrust to upper crust (~0.01 and 15 MPa/km depth, respectively, e.g., Marone [1991]; Blanpied *et al.* [1995]). Given these parameter values, the value of (A-B) should increase linearly from 0 to 4 MPa in the crust. If we assume a uniform effective normal stress of 50 MPa below 2.5 km depth (following Lapusta *et al.,* 2000), then (A-B) should be 0.5 MPa throughout the crust, which is in better agreement with our findings. Thus, low (A-B) could indicate that σ_n' in the crust is small (~50 MPa) because of elevated hydraulic pressures in the shear zone. Alternately, if we assume more typical pore pressures in the crust, the low (A-B) could mean that (a-b) is smaller than what the laboratory studies suggest (e.g., [a-b] = 0.001 − 0.003 rather than 0.01 in the upper to middle crust). Our finding that a low (A-B) is required to reproduce observed İzmit earthquake postseismic deformation is consistent with the study of Linker and Rice (1997), whose models require a uniform (A-B) of 0.5 MPa to explain postseismic deformation following the 1989 Loma Prieta, California, earthquake.

A weakly velocity-strengthening fault zone penetrating through the middle crust is also consistent with significant coseismic slip below 15 km, which is required by our elastically layered coseismic model. (A more strongly velocity-strengthening material below the seismogenic zone would have prevented much downward propagation of the rupture.) Frictional slip laws with two state variables (e.g., Blanpied *et al.,* 1998) could be responsible for such weakly velocity-strengthening conditions in the middle crust (i.e., at temperatures of less than ~500°C).

We have examined the possibility that our use of large model elements might have caused us to underestimate (A-B). The concern was that if we used a smaller nodal spacing, we might better capture high shear stresses at interfaces between high and low coseismic slip patches, which could lead to larger estimates of (A-B). We ran test models of a simple M_w 7.4 strike-slip earthquake with uniform slip on a straight fault, using 2- and 6-km-thick elements in the upper to middle crust. The more finely discretized model yielded a maximum shear stress of 10 MPa just below the rupture (over twice that of the more coarsely discretized model), but shear stress decreased more markedly with depth. Characteristic

decay times for near-field surface velocities were smaller for the more finely discretized case (<10 days versus ~60 days) because once the narrow, high-stress interval below the rupture had slipped, shear stresses remaining on the structure were too low to maintain afterslip at a remotely comparable rate. However, similar values of (*A*-*B*) yielded similar total postseismic displacements. As the İzmit earthquake postseismic displacements are characterized by both a transient with $t_c$equal to 80 days and (locally) a smaller amplitude transient with a decay time of hours, we suggest that the distribution of coseismic slip overall was probably fairly smooth (as shown by Reilinger *et al.,* 2000) and that our elements adequately represent the spatial variation of slip (and coseismic shear stress) over most of the fault. However, localized fault patches with high coseismic shear stress may be responsible for the $t_c < 12$ hr velocity transient.

Sensitivity of Coulomb Stress Estimates to Model and GPS Data Errors

There are two major sources of error in our Coulomb stress estimates. First, a model that fits surface displacement data within small tolerances may be nonunique. Different models that fit surface displacements reasonably well may yield significantly different Coulomb stress estimates. The most obvious example of this is our finding that a layered elastic model with extra slip below 9 km that matches coseismic surface displacements as well as the uniform elastic model yields far greater coseismic Coulomb stresses in the near field.

Another potential source of large errors in crustal stress estimates arises from the fact that though different models yield distinct deformation patterns, the differences may be too small to detect with GPS data, particularly from campaign-mode sites with few occupations. For example, models of linear viscous creep, viscoelastic lower crust relaxation, and frictional afterslip give surface displacements at many Marmara Sea region campaign-mode sites that are distinct, yet are within the 95% confidence limits for displacement measurements (i.e., two times the one-sigma values in Table 1). However, these models give significantly different postseismic stress changes at Marmara region reference points A–D (Fig. 14). Although the models we examine produce distinct displacement fields, we may only distinguish between them if the 95% confidence limits for horizontal displacements (at least at some stations) are less than about 5 mm. We may choose a preferred model and estimate postseismic stressing on Marmara Sea faults with some confidence, chiefly because of the small error ranges associated with continuous GPS stations in the area.

Modeling the time decay of surface deformation is crucial to the understanding of the dynamics of postseismic deformation. Models that fit surface displacements equally well over a particular time epoch may perform differently over a different time interval. For example, models of all the three classes that we evaluate may be devised to fit the measured postseismic displacements prior to the Düzce earthquake about equally well (though when misfit is weighted by measurement error, the frictional afterslip model is favored). However, the best-fitting viscoelastic lower crust model predicts less surface velocity decay with time than the other two models. Three hundred days after the İzmit earthquake, this model yields displacements that are too large in the intermediate to far-field (e.g., Fig. 13, stations KANT and ULUT). Long-term monitoring at the intermediate- to far-field GPS sites is thus invaluable for discerning between models.

The Future

Without accounting for stress contributions from the Düzce event, our favored model predicts that measurable postseismic deformation (i.e., >2 mm/yr) caused by afterslip should cease at most GPS site locations within about 5 yr. The duration of observable postseismic deformation caused by afterslip (and/or linear viscous shear zone creep) depends on (1) how long it takes to relieve coseismic shear loading of the fault surface and (2) for velocity-strengthening frictional slip, how long the rupture surface remains velocity-strengthening. If greater postseismic surface velocities persist over the next several years, relaxation of viscoelastic lower crust or upper mantle will likely be the cause.

Figure 15 illustrates the decay in shear stress on the İzmit rupture surface during the first 300 days after the İzmit earthquake. Our modeling suggests that afterslip has released about 90% of the total available coseismic shear strain energy on the NAFZ (somewhat less for the layered elastic model). This means that most of the afterslip that can occur has occurred. Much of the residual shear stress is concentrated at depths of less than 15 km off the fault ends, where velocity-weakening conditions likely prevail. Residual shear stresses in the upper crust east of the İzmit rupture were probably relieved by the Düzce event. The western end of the coseismic rupture (Yalova segment) was coseismically loaded by up to 1 MPa, and shear stresses increased there by another ca. 0.2 MPa during the first 300 days after the İzmit earthquake.

Both coseismic and postseismic slip have loaded the lower crust and upper mantle. Viscoelastic relaxation in response to this loading should continue for years or decades, though the rate of such relaxation (and associated upper crustal deformation) is uncertain. In parts of western Turkey, seismic data indicate that low-density, quartz-bearing rock comprises the lower crust, and surface heat flow data suggest that this lower crust is hot (Mindavelli and Mitchell, 1989; Mueller *et al.,* 1997; Pfister *et al.,* 1997; Saunders *et al.,* 1998). Such lower crust could relax over short timescales, so we may see the effects of viscoelastic relaxation in this region within the next few years. On the other hand, sharp gradients in secular velocities across NAFZ segments in western Turkey and the Marmara region may suggest that the lower crust in this region is interseismically strong (B. H.

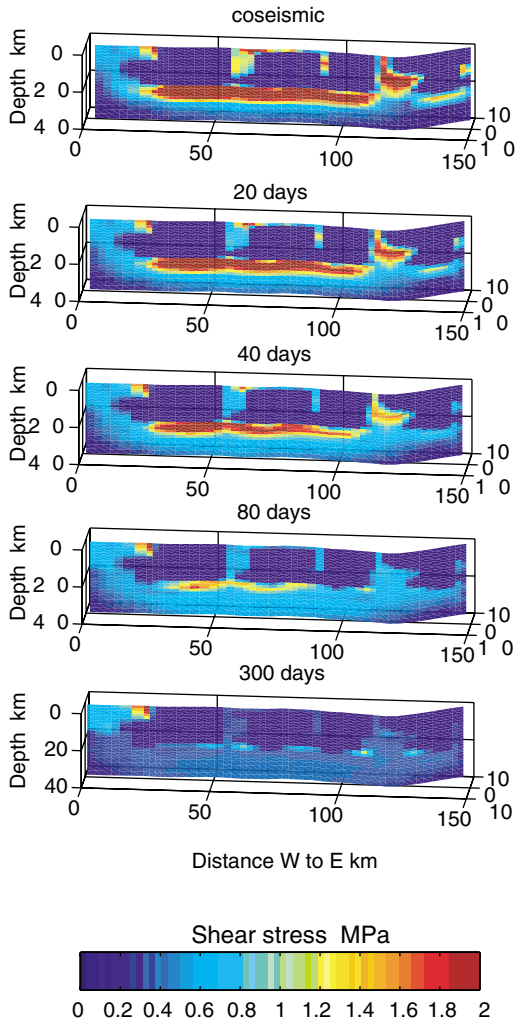

Figure 15. Shear stress evolution on and below the İzmit rupture up to 300 days after the earthquake, from our favored frictional afterslip model. Not considering stress changes accompanying the Düzce earthquake, about 90% of the coseismic loading has been relieved. This suggests that continued afterslip or creep at depth on the NAFZ would produce only modest (but broadly distributed) postseismic deformation.

Hager, 2000, personal comm.) and that viscoelastic relaxation of the lower crust during the next few years should be insignificant. Continued monitoring of the postseismic deformation of the İzmit earthquake will allow us to distinguish between these two views and will teach us a great deal about crustal rheology and the evolution of seismic hazard in western Turkey.

Conclusions

İzmit earthquake postseismic deformation prior to the Düzce earthquake was caused by the afterslip on and below the coseismic rupture. Regardless of how this slip or creep is modeled, it is concentrated around the hypocenter and on the western Karadare segment, where coseismic slip is low and the fault zone is coseismically loaded. Our frictional afterslip model has the added advantage of producing significant afterslip on the rupture surface in the upper crust but only minor afterslip on the Yalova segment, and thus explains the main features of afterslip inversions presented in our co-author's article (Bürgmann *et al.,* 2002). This model also reproduces time-dependent GPS displacements better than the competing models in the Marmara region, in the near field, and at the continuous GPS stations.

Our best frictional afterslip model requires that $(A\text{-}B) = (a\text{-}b)\,\sigma_n' = 0.2$ MPa (0.4 MPa for a more realistic, layered elastic structure). Our result suggests either high pore pressure (and thus low σ_n') in the NAFZ at depth or a low $(a\text{-}b)$ value (<0.005) at depths exceeding a few kilometers.

The coseismic Coulomb stress change at the Düzce hypocenter caused by the İzmit earthquake (for right-lateral slip on a surface dipping 50° N) was at least 0.14 MPa. Before the Düzce earthquake, another 0.1 MPa of Coulomb stress accumulated at the hypocenter. Over the first 300 days after the earthquake, postseismic Coulomb stresses on the Marmara fault within about 160 km of the rupture were about 15%–25% of the coseismic value (Fig. 14). Three hundred days after the earthquake, postseismic stressing rates on the NAFZ in the Marmara region declined to values equal to or less than the secular Coulomb stressing rate (0.01 MPa/yr). Our Marmara region Coulomb stress estimates are well constrained by continuous GPS data, which clearly allow little or no postseismic slip along the Yalova segment or further west.

Afterslip has released about 90% of the coseismic shear loading on the NAFZ. Much of the remaining strain energy is deep in the crust and in the seismogenic zone beyond the west end of the rupture. We anticipate that postseismic deformation will continue at a low rate in the Marmara region, because of viscoelastic relaxation of the lower crust and limited afterslip or viscous creep at depth on the NAFZ.

In conclusion, we wish to point out the importance of incorporating layered elastic structure in dynamic postseismic deformation models, especially when the goal is to estimate fault-zone rheology or constitutive relations. Detailed modeling of postseismic slip relies heavily on the driving (coseismic) stresses, which are severely affected by elastic layering. We also caution that uniform elastic models that correctly reproduce coseismic surface displacements may significantly underestimate Coulomb stress changes on the nearby faults.

Acknowledgments

This research was funded by NSF grants INT 00001143 and EAR 9909730. We thank Jim Rice for his thoughtful review of this manuscript. We are also grateful to Bob King, Tom Herring, Simon McClusky, and Brad Hager for providing their insights on GPS data analysis and crustal deformation.

References

Ayhan, M. E., R. Bürgmann, S. McClusky, O. Lenk, B. Aktug, E. Herece, and R. E. Reilinger (2001). Kinematics of the $M_w = 7.2$, 12 November 1999, Düzce, Turkey Earthquake, *Geophys. Res. Lett.* **28,** 367–370.

Bechor, N., P. Segall, K. M. Johnson, Y. Hsu, and S. B. Yu (2001). Postseismic slip following the 1999 Chi-Chi, Taiwan, earthquake, *Seism. Res. Lett.* **72,** 248.

Blanpied, M. L., D. A. Lockner, and J. D. Byerlee (1991). Fault stability inferred from granite sliding experiments at hydrothermal conditions, *Geophys. Res. Lett.* **18,** 609–612.

Blanpied, M. L., D. A. Lockner, and J. D. Byerlee (1995). Frictional slip of granite at hydrothermal conditions, *J. Geophys. Res.* **100,** 13,045–13,064.

Blanpied, M. L., C. J. Marone, D. A. Lockner, J. D. Byerlee, and D. P. King (1998). Quantitative measure of the variation in fault rheology due to fluid-rock interactions, *J. Geophys. Res.* **103,** 9691–9712.

Bouchon, M., M. N. Toksöz, H. Karabulut, M. P. Bouin, M. Dietrich, M. Aktar, and M. Edie (2002). Space and time evolution of rupture and faulting during the 1999 İzmit (Turkey) earthquake, *Bull. Seism. Soc. Am.* **92,** no. 1, 256–266.

Bürgmann, R., S. Ergintav, P. Segall, E. Hearn, S. McClusky, R. Reilinger, H. Woith, and J. Zschau (2002). Time-space variable afterslip on and deep below the İzmit earthquake rupture, *Bull. Seism. Soc. Am.* **92,** no. 1, 126–137.

Bürgmann, R., M. G. Kagan, V. E. Levin, C. H. Scholz, R. W. King, and G. M. Steblov (2001). Rapid aseismic moment release following the 5 December 1997 Kronotsky, Kamchatka, earthquake, *Geophys. Res. Lett.* **28,** 1331–1334.

Carter, N. L., and M. C. Tsenn (1987). Flow properties of continental lithosphere, *Tectonophysics* **136,** 27–63.

Delouis, B., D. Giardini, P. Lundgren, and J. Salichon (2002). Joint inversion of InSAR, GPS, teleseismic, and strong-motion data for the spatial and temporal distribution of earthquake slip: application to the 1999 İzmit mainshock, *Bull. Seism. Soc. Am.* **92,** no. 1, 278–299.

Dieterich, J. H. (1979). Modeling of rock friction 1. Experimental results and constitutive equations, *J. Geophys. Res.* **84,** 2161–2168.

Ergintav, S., R. Bürgmann, S. McClusky, R. Çakmak, R. E. Reilinger, O. Lenk, A. Barka, and H. Özener (2002). Postseismic deformation near the İzmit earthquake (17 August 1999, *M* 7.5), rupture zone, *Bull. Seism. Soc. Am.* **92,** no. 1, 194–207.

Feigl, K. L., F. Sarti, H. Vadon, S. McClusky, S. Ergintav, R. Bürgmann, A. Rigo, P. Durand, D. Massonet, and R. Reilinger (2002). Estimating slip distribution for the İzmit mainshock from coseismic GPS, ERS-1, RADARSAT, and SPOT measurements, *Bull. Seism. Soc. Am.* **92,** no. 1, 138–160.

Gülen, L., A. Pınar, D. Kalafat, N. Özel, G. Horasan, M. Yılmazer, and A. Işıkara (2002). Surface fault breaks, aftershock distribution, and rupture process of the 17 August 1999 İzmit, Turkey earthquake, *Bull. Seism. Soc. Am.* **92,** no. 1, 230–244.

Hanmer, S. (1988). Great Slave Lake shear zone, Canadian Shield: reconstructed vertical profile of a crustal scale fault zone, *Tectonophysics* **149,** 245–264.

Hansen, F., and N. Carter (1983). Semibrittle creep of dry and wet Westerly Granite at 1000 MPa, in *Proc. of the 24th U.S. Symposium on Rock Mechanics,* Texas A & M University, College Station, Texas, 429–447.

Heki, K., S. Miyazaki, and H. Tsuji (1997). Silent fault slip following an interplate thrust earthquake at the Japan Trench, *Nature* **386,** 595–598.

Honkura, Y., A. M. Isikara, N. Oshiman, B. Ücer, S. Baris, M. K. Tuncer, M. Matsushima, R. Pektas, C. Celik, S. B. Tank, F. Takahashi, M. Nakanishi, R. Yoshimura, Y. Ikeda, and T. Komut (2000). Preliminary results of multidisciplinary observations before, during, and after the Kocaeli (İzmit) earthquake in the western part of the North Anatolian Fault Zone, *Earth Planets Space* **52,** 293–298.

Hubert-Ferrari, A., A. Barka, E. Jacques, S. Nalbant, B. Meyer, R. Armijo, P. Tapponnier, and G. C. P. King (2001). Seismic hazard in the Marmara Sea region following the 17 August 1999 İzmit earthquake, *Nature* **404,** 269–273.

Jaoul, O., J. Tullis, and A. Kronenburg (1984). The effect of varying water contents on the creep behaviour of Heavitree quartzite, *J. Geophys. Res.* **89,** 4298–4312.

Kruse, S., M. K. McNutt, J. Phipps-Morgan, L. Royden, and B. P. Wernicke (1991). Lithosphere extension near Lake Mead Nevada: a model for ductile flow in the lower crust, *J. Geophys. Res.* **96,** 4435–4456.

Lapusta, N., J. R. Rice, Y. Ben-Zion, and G. Zheng (2000). Elastodynamic analysis for slow tectonic loading with spontaneous rupture episodes on faults with rate-and state-dependent friction, *J. Geophys. Res.* **105,** 23,765–23,789.

Li, V. C., and J. R. Rice (1987). Crustal deformation in great California earthquake cycles, *J. Geophys. Res.* **92,** 11,533–11,551.

Linker, M., and J. Rice (1997). Models of postseismic deformation and stress transfer associated with the Loma Prieta earthquake, in *U.S. Geological Survey Paper 1550-D: The Loma Prieta, California Earthquake of October 17, 1989: Aftershocks and Postseismic Effects,* D253–D275.

Marone, C. J., C. H. Scholz, and R. Bilham (1991). On the mechanics of earthquake afterslip, *J. Geophys. Res.* **96,** 8441–8452.

McClusky, S., S. Balassanian, A. Barka, C. Demir, S. Ergintav, I. Georgiev, O. Gurkan, M. Hamburger, K. Hurst, H. Kahle, K. Kastens, G. Kekelidze, R. King, V. Kotzev, O. Lenk, S. Mahmoud, A. Mishin, M. Nadariya, A. Ouzounis, D. Paradissis, Y. Peter, M. Prilepin, R. Reilinger, I. Sanli, H. Seeger, A. Tealeb, M. N. Toksöz, and G. Veis (2000). Global positioning constraints on plate kinematics and dynamics in the Eastern Mediterranean and Caucasus, *J. Geophys. Res.* **105,** 5695–5719.

Meade, B., B. Hager, S. McClusky, R. Reilinger, S. Ergintav, O. Lenk, A. Barka, and H. Özener (2002). Estimates of seismic potential in the Marmara Sea region from block models of secular deformation constrained by GPS measurements, *Bull. Seism. Soc. Am.* **92,** no. 1, 208–215.

Melosh, H. J., and A. Raefsky (1981). A simple and efficient method for introducing faults into finite element computations, *Bull. Seism. Soc. Am.* **71,** 1391–1400.

Mindavelli, O., and B. Mitchell (1989). Crustal structure and possible anisotropy in Turkey from seismic surface wave dispersion, *Geophys. J. Int.* **98,** 93–106.

Mooney, W. D., G. Laske, and G. Masters (1998). CRUST 5.1: a global crustal model at $5^\circ \times 5^\circ$, *J. Geophys. Res.* **103,** 727–747.

Mueller, S., H.-G. Kahle, and A. Barka (1997). Plate tectonic situation in the Anatolian-Aegean region, in *Active Tectonics of Northwestern Anatolia-The MARMARA Poly-Project*, C. Schindler and M. Pfister (Editors), vdf. Hochschulverlag, AG on der ETH Zürich, 13–28.

Onsel, A. O., and M. Wyss (2000). The major asperities of the $M_w = 7.4$ İzmit earthquake defined by the microseismicity of the two decades before it, *Geophys. J. Int.* **143,** 501–506.

Parsons, T., S. Toda, R. S. Stein, A. Barka, and J. H. Dieterich (2001). Heightened odds of large earthquakes near Istanbul: an interaction-based probability calculation, *Science* **288,** 661–665.

Peltzer, G., P. Rosen, F. Rogez, and K. Hudnut (1998). Poroelastic rebound along the Landers 1992 earthquake surface rupture, *J. Geophys. Res.* **103,** 30,131–30,145.

Pfister, M., W. Balderer, E. Greber, H.-G. Kahle, D. Mayer-Rosa, S. Mueller, L. Rybach, C. Schindler, S. Sellami, and C. Straub (1997). Synthesis of the MARMARA poly-project, in *Active Tectonics of Northwestern Anatolia-The MARMARA Poly-Project,* C. Schindler and M. Pfister (Editors), 539–565.

Pollitz, F. F., G. Peltzer, and R. Bürgmann (2000). Mobility of continental mantle: evidence from postseismic geodetic observations following the 1992 Landers earthquake, *J. Geophys. Res.* **105,** 8035–8054.

Reilinger, R., S. Ergintav, R. Bürgmann, S. McCluskey, O. Lenk, A. Barka, O. Gurkan, E. Hearn, K. L. Feigl, R. Cakmak, B. Aktug, H. Ozener,

and M. N. Toksöz (2000). Coseismic and postseismic fault slip for the 17 August 1999, $M = 7.5$, İzmit, Turkey Earthquake, *Science* **289,** 1519–1524.

Roeloffs, E. (1996). Poroelastic techniques in the study of earthquake-related hydrologic phenomena, *Adv. Geophys.* **37,** 135–195.

Roy, M., and L. Royden (2000). Crustal rheology and faulting at strike-slip plate boundaries 2. Effects of lower crustal flow, *J. Geophys. Res.* **105,** 5599–5613.

Ruina, A. L. (1983). Slip instability and state variable friction laws, *J. Geophys. Res.* **88,** 10,359–10,370.

Rybicki, K. (1971). The elastic residual field of a very long strike-slip fault in the presence of a discontinuity, *Bull. Seism. Soc. Am.* **61,** 79–92.

Saucier, F., and E. D. Humphreys (1993). Horizontal crustal deformation in Southern California from joint models of geologic and very long baseline interferometry measurements, in *Contributions of Space Geodesy to Geodynamics*, D. E. Smith and D. L. Turcotte (Editors), Vol. 23, American Geophysical Union, Geodynamics Series, Washington D.C., 139–176.

Saunders, P., K. Priestley, and T. Taymaz (1998). Variations in the crustal structure beneath western Turkey, *Geophys. J. Int.* **134,** 373–389.

Savage, J. C. (1987). Effect of crustal layering upon dislocation modeling, *J. Geophys. Res.* **92,** 10,595–10,600.

Savage, J. C., and W. H. Prescott (1978). Asthenosphere readjustment and the earthquake cycle, *J. Geophys. Res.* **83,** 3369–3376.

Savage, J. C., and J. L. Svarc (1997). Postseismic deformation associated with the 1992 $M_w = 7.3$ Landers earthquake, southern California, *J. Geophys. Res.* **102,** 7565–7577.

Sibson, R. H. (1983). Continental fault structure and the shallow earthquake source, *J. Geol. Soc. Lond* **140,** 741–767.

Stesky, R. M. (1978). Mechanics of high temperature frictional sliding of Westerly granite, *Can. J. Earth Sci.* **15,** 361–375.

Straub, C., H.-G. Kahle, and C. Schindler (1997). GPS and geologic estimates of the tectonic activity in the Marmara Sea Region, NW Anatolia, *J. Geophys. Res.* **102,** 27,587–27,601.

Tse, S. T., and J. R. Rice (1986). Crustal earthquake instability in relation to the depth variation of frictional slip properties, *J. Geophys. Res.* **91,** 9452–9472.

Tsenn, M. C., and N. L. Carter (1987). Upper limits of power-law creep of rocks, *Tectonophysics* **136,** 1–26.

Vichnevetsky, R. (1981). *Computer Methods for Partial Differential Equations, Volume 1: Elliptic Equations and the Finite-Element Method,* in *Prentice-Hall Series in Computational Mathematics,* Cleve Moler, (Advisor), Prentice Hall, Inc, Englewood Cliffs, New Jersey.

Wang, J., B. Hobbs, A. Ord, T. Shimamoto, and M. Toriumi (1994). Newtonian dislocation creep in quartzites: implications for the rheology of the lower crust, *Science* **265,** 1204–1205.

Wright, T., E. Fielding, and B. Parsons (2001). Triggered slip: observations of the 17 August 1999 İzmit (Turkey) earthquake using radar interferometry, *Geophys. Res. Lett.* **28,** 1079–1082.

Wyatt, F. K., D. C. Agnew, and M. Gladwin (1994). Continuous measurements of crustal deformation for the 1992 Landers earthquake sequence, *Bull. Seism. Soc. Am.* **84,** 768–779.

Department of Earth, Atmospheric, and Planetary Sciences
54-614, Massachusetts Institute of Technology
Cambridge, Massachusetts 02139
lizh@chandler.mit.edu
(E.H.H.)

Department of Earth and Planetary Sciences
University of California at Berkeley
Berkeley, California 94720
burgmann@seismo.berkeley.edu
(R.B.)

Earth Resources Laboratory
Massachusetts Institute of Technology
Cambridge, Massachusetts 02142
reilinge@erl.mit.edu
(R.E.R.)

Manuscript received 22 September 2000.